Published by Institute of Physics Publishing for SISSA/ISAS

Received: *March 5, 2002*
Revised: *April 29, 2002*
Accepted: *May 3, 2002*

# The contribution of the four-parton final states to $\gamma^*\gamma^* \to$ hadrons

**Vittorio Del Duca**

*Istituto Nazionale di Fisica Nucleare, Sez. di Torino*
*via P. Giuria, 1 - 10125 Torino, Italy*
*E-mail:* delduca@to.infn.it

**Fabio Maltoni**

*Dept. of Physics, University of Illinois at Urbana-Champaign*
*Urbana, IL 61801, USA*
*E-mail:* maltoni@uiuc.edu

**Zoltán Trócsányi***

*University of Debrecen and*
*Institute of Nuclear Research of the Hungarian Academy of Sciences*
*H-4001 Debrecen, PO Box 51, Hungary*
*E-mail:* zoltan@zorro.atomki.hu

Abstract: In the analysis of the total cross section for the $\gamma^*\gamma^* \to$ hadrons process, we include the four parton final states, which are part of the $\mathcal{O}(\alpha_S^2)$ corrections. The four-parton final states contain the diagrams with gluon exchange in the crossed channel, which constitute the leading order of the BFKL resummation. We show that the diagrams with gluon exchange in the crossed channel play an important role in the large $Y$ region, however their contribution to the cross section must be evaluated exactly. In fact, the high-energy limit, which constitutes the kinematic framework of the BFKL resummation, is not sufficiently accurate at LEP2 energies. The inclusion of the diagrams with gluon exchange in the crossed channel reduces the discrepancy between the theory and the LEP2 data collected by the L3 Collaboration, but the data still lie above the theory, even allowing for a large scale uncertainty in the theory. Thus, in order to describe accurately the data for $\gamma^*\gamma^* \to$ hadrons in the large $Y$ region, corrections of an order higher than $\mathcal{O}(\alpha_S^2)$ seem to be necessary.

Keywords: QCD, NLO Computations, Jets.

*Széchenyi fellow of the Hungarian Ministry of Education

## Contents



## 1. Introduction

Strong interaction processes, characterised by a large kinematic scale, are described in perturbative QCD by a fixed-order expansion of the parton cross section in $\alpha_S$, complemented, if the scattering process is initiated by strong interacting partons, with the Altarelli-Parisi evolution of the parton densities. However, in kinematic regions characterised by two very different hard scales, a fixed-order expansion might not suffice: large logarithms of the ratio of the kinematic scales appear, which may have to be resummed. In processes where the centre-of-mass energy $s$ is much larger than the typical momentum transfer $t$, the sub-process which features gluon exchange in the crossed channel, and that usually appears at $\mathcal{O}(\alpha_S^2)$, tends to dominate over the other sub-processes. That sub-process constitutes the leading-order term of the BFKL equation, which is an equation for the Green's function of gluon exchanged in the crossed channel. The BFKL equation [1, 2, 3] resums the logarithms of type $\ln(s/|t|)$.

Over the last decade, several observables, like the scaling violations of the $F_2$ structure function [4, 5], forward-jet production in DIS [6]–[11], dijet production at large rapidity intervals [12]–[19], and $\gamma^*\gamma^* \to$ hadrons in $e^+e^-$ collisions [20]–[26] have been proposed in the literature as candidates for the detection of the BFKL evolution, and have been



JHEP05(2002)005

measured and analysed as functions of observables, which aim to single out large logarithms of type $\ln(s/|t|)$. However, from a phenomenological point of view, in order to claim detection of BFKL gluon radiation in a given process in an unambiguous way, we must rule out any explanation of that process in terms of a fixed order expansion, or in terms of a different resummation. Thus, in order to make a sound BFKL analysis, we must ascertain first of all if:

- the sub-process with gluon exchange in the crossed channel, i.e. the leading order of the BFKL resummation, dominates over all the other sub-processes;
- the acceptance cuts of the experiment under consideration allow us to reach the kinematic region of the high-energy limit, where the approximations needed for a BFKL analysis are valid.

The goal of this paper is to analyse whether the two conditions above are fulfilled in the $\gamma^*\gamma^* \to$ hadrons process at LEP2. Namely, we consider

$$\gamma^* + \gamma^* \;\longrightarrow\; \text{hadrons}, \tag{1.1}$$

in $e^+e^-$ collisions at photon virtualities $q_i^2 = -Q_i^2 < 0$, and for large centre-of-mass energies squared $W^2 = (q_1 + q_2)^2$, with $q_i$ being the momenta of the photons. In practice we can realise the scattering (1.1) in the process

$$e^+ + e^- \;\longrightarrow\; e^+ + e^- + \text{hadrons}, \tag{1.2}$$

of which eq. (1.1) constitutes a subset. Other contributions to the process in eq. (1.2) are, for example, those in which the incoming $e^+e^-$ pair annihilates into a photon or a $Z$ boson, eventually producing the hadrons and a lepton pair, or those in which one (or both) of the two photons is replaced by a $Z$ boson. However, it is not difficult to devise a set of cuts such that the multiperipheral process

$$e^+ + e^- \;\longrightarrow\; e^+ + e^- + \underbrace{\gamma^* + \gamma^*}_{\longrightarrow\ \text{hadrons}}, \tag{1.3}$$

gives the only non-negligible contribution to the process in eq. (1.2). One can tag both of the outgoing leptons, and retain only those events (thus termed *double-tag events*) in which the scattering angles of the leptons are small: in such a way, the contamination due to annihilation processes is safely negligible. Furthermore, small-angle tagging also guarantees that the photon virtualities are never too large (at LEP2, one typically measures $Q_i^2 \approx 10\,\mathrm{GeV}^2$); therefore, the contributions from processes in which a photon is replaced by a $Z$ boson are also negligible. Thus, it is not difficult to extract the cross section of the process $\gamma^*\gamma^* \to$ hadrons from the data relevant to the process in eq. (1.2). Double-tag events have in fact been studied by the CERN L3 and OPAL Collaborations, at various $e^+e^-$ centre-of-mass energies ($\sqrt{s} = 91$ and 183 GeV [20], and 189-202 GeV [21, 22]).

The process (1.1) has been analysed at leading order [28] and at next-to-leading order [29] (NLO) in $\alpha_S$. However, at the high end of the $W$ spectrum, the NLO prediction does not suffice to describe the data. In this paper, we consider the part of the next-to-next-to-leading order (NNLO) corrections which yields the dominant contribution to the total cross section in the large-$W$ region. As we shall argue below, that contribution comes from four quark final states. Since four parton final states do not yield *per se* a finite contribution to the total cross section, we consider a subset of them, those with gluon exchange in the crossed channel, which are finite, and argue that they yield the most important contribution to the total cross section in the large-$W$ region.

The paper is organised as follows: in section 2 we set the theoretical framework; in section 3 we consider the four-quark contribution to the $\mathcal{O}(\alpha_S^2)$ corrections, exactly and in the high-energy limit; analysing various theoretical predictions for rapidity and $W$ distributions in section 4, we substantiate our claim that the most important contribution to the total cross section in the large-$W$ region comes from four-quark production with gluon exchange in the crossed channel, and also show that the high-energy limit is not sufficiently accurate at LEP2 energies; in section 5 we present our phenomenological results, by comparing our predictions to the L3 data [22] (we shall not perform a comparison with the OPAL data, which have much poorer statistics); in section 6 we draw our conclusions.

## 2. The theoretical framework

At leading order, the multiperipheral process (1.3) is modelled by the partonic subprocess $\gamma^*\gamma^* \to q\bar{q}$, depicted in figure 1$a$, which has been computed for massless and massive final-state fermions [28]. In ref. [29] the $\mathcal{O}(\alpha_S)$ QCD corrections to the process (1.3) were computed for final-state massless quarks (sample diagrams are given in figure 1$b$–$c$). However, the NLO analysis of ref. [29] yields a cross section behaving as

$$\sigma_{\gamma^*\gamma^*} \sim \frac{1}{W^2}\,, \tag{2.1}$$

modulo logarithmic corrections. Thus, it is only propaedeutic to the BFKL resummation, whose leading-order term is based on the exchange of a gluon in the crossed channel, which appears only at $\mathcal{O}(\alpha_S^2)$ (figure 1$d$). The BFKL resummation then builds up gluon emission along the gluon exchanged in the crossed channel (the first rungs of the ladder are represented in figure 1$e$–$f$). The diagrams represented by figure 1$d$ are expected to yield a cross section which, away from the threshold and the kinematic limit, is weakly dependent on $W$. The additional gluon emissions build up the logarithmic corrections which the BFKL theory resums, so that the full cross section is expected to behave as

$$\sigma_{\gamma^*\gamma^*} \sim \sum_{j=0}^{\infty} a_{0j}\alpha_S^j + a_1\alpha_S^2\sum_{j=0}^{\infty}(\alpha_S L)^j + a_2\alpha_S^2\sum_{j=0}^{\infty}\alpha_S(\alpha_S L)^j \; + \cdots\,, \tag{2.2}$$

where $L = \log(W^2/\mu_{\rm W}^2)$ is a large logarithm, and the quantity $\mu_{\rm W}^2$ is a mass scale squared, typically of the order of the crossed-channel momentum transfer and/or of the photon virtualities. In eq. (2.2), the second and third sums collect the contributions which feature *only* gluon exchange in the crossed channel, the second (third) sum resumming the BFKL (next-to-)leading logarithmic corrections; the $a_1$, $a_2$ coefficients behave like $1/\mu_{\rm W}^2$. The

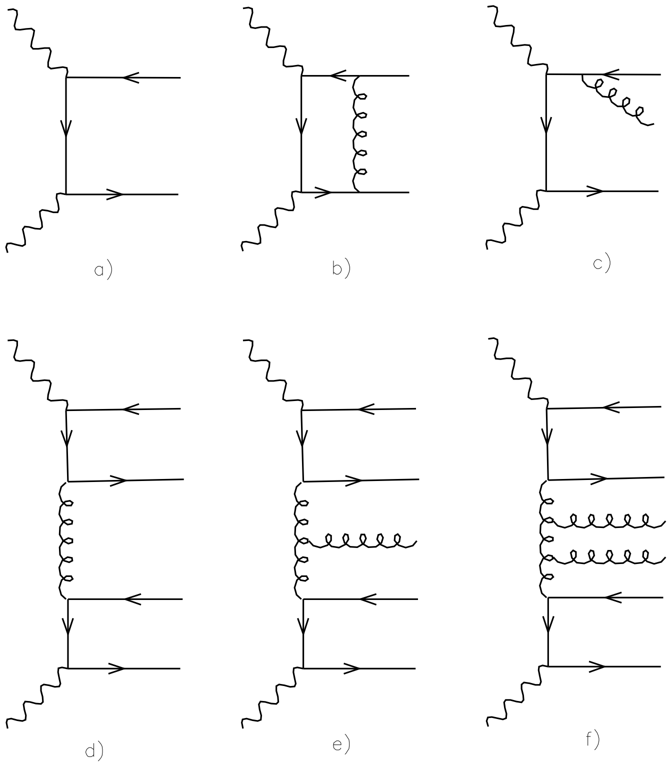


**Figure 1:** Sample of diagrams contributing to the production of hadrons in the collision of two off-shell photons.

ellipses refer to logarithmic corrections beyond the next-to-leading accuracy. The first sum in eq. (2.2) is a fixed-order expansion in $\alpha_S$ starting at $\mathcal{O}(\alpha_S^0)$, and collects the contributions which do not feature gluon exchange in the crossed channel; the $a_{0j}$ coefficients behave like $1/W^2$.[1] Thus, it is clear that the second and third sums of eq. (2.2) will eventually dominate over the first sum in the asymptotic energy region $W \to \infty$. The second sum of eq. (2.2) has been analysed in the region $W^2 \gg \mu_{\mathrm{W}}^2$, by computing in the high-energy limit the $a_1$ coefficient in the massless [25, 26] and in the massive [27] case. As mentioned above, the $a_{00}$ term in the first sum has been computed in ref. [28] for massless and massive final-state quarks, while the $a_{01}$ term has been computed in ref. [29], for massless final-state quarks. In the next paragraph, we shall illustrate that at present a calculation of the $a_{02}$ term is unfeasible. In this work, we compute *exactly* the $a_1$ coefficient in the massless limit, and add it to the $a_{00}$ and $a_{01}$ terms. However, we do not perform the resummation, i.e. we consider only the $j = 0$ term in the second sum of eq. (2.2).

In examining the radiative corrections to the process (1.3), we first note that at present a calculation of the full $\mathcal{O}(\alpha_S^2)$ corrections to the total and to the inclusive jet and dijet cross sections is unfeasible, since it would require a computation of two-loop amplitudes,

[1] The $a_{02}$ coefficient may feature terms which behave like $1/(W\mu_{\mathrm{W}})$ and arise from the interference between diagrams with gluon exchange in the crossed channel and diagrams with quark exchange in the crossed channel. These interference terms have been analysed in section 4 (see the discussion of figure 3).

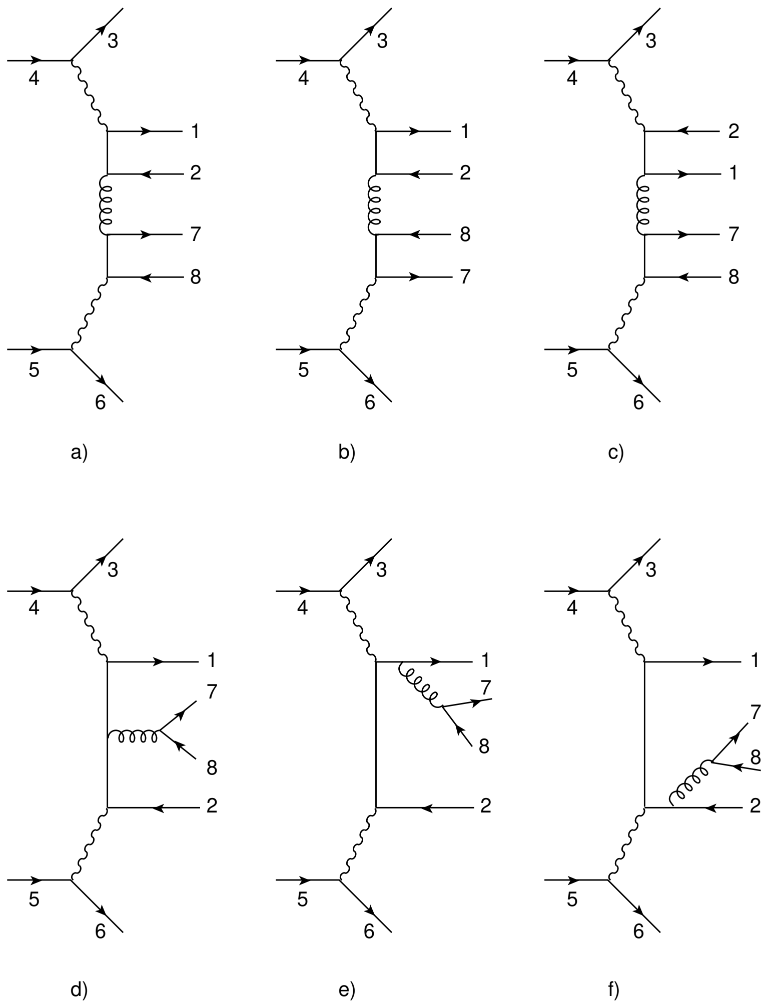


**Figure 2:** Amplitude for $e^+e^- \to e^+e^-\gamma^*\gamma^* \to e^+e^-q\bar{q}Q\bar{Q}$ scattering. Figures ($a$), ($b$) and ($c$) correspond to the functions $g_a$, $g_b$ and $g_c$ in eq. (3.3); figures ($d$), ($e$) and ($f$) contribute to the function $f$.

including double box diagrams with two off-shell legs which are not known. A calculation of the $\mathcal{O}(\alpha_S^2)$ corrections to the inclusive three-jet rate is feasible but difficult, and given the very limited experimental statistics available it would have at present only an academic value. Therefore, we shall limit ourselves to the analysis of the contribution of the four parton final states to the $\mathcal{O}(\alpha_S^2)$ corrections. In particular, the final states can be made of either two quark pairs or a quark pair and two gluons. In figure 2 the diagrams with two final-state quark pairs are represented.

The treatment of the four parton final states poses some additional problems, because as far as the total, the inclusive jet and the dijet cross sections are concerned, only the contribution of the four-quark diagrams with gluon exchange in the crossed channel (figure 2$a$–$c$) is infrared finite. Henceforth, we shall term the diagrams with gluon exchange in the crossed channel the $g$ *class*. The diagrams of the $g$ class are by themselves gauge invariant and as described in the former paragraph, they are expected to yield a cross section which is only logarithmically dependent on $W^2$. Thus, as $W^2$ grows, they are expected to dominate over the diagrams with quark exchange in the crossed channel. The diagrams with two final-state quark pairs and quark exchange in the crossed channel (figure 2$d$–$f$) and the diagrams with a quark pair and two gluons in the final state, present infrared divergences when one or both the final-state gluons become collinear to the parent quarks or between themselves, when two or three final-state quarks become collinear, or when the gluon emitting the quark pair becomes soft. We shall term the diagrams with a quark pair and two gluons in the final state, and the diagrams with two final-state quark pairs and quark exchange in the crossed channel the *f class*. The diagrams of the $f$ class would all be part of the proper NNLO corrections to the process $\gamma^*\gamma^* \to q\bar{q}$, and after cancellation of their infrared divergences by the corresponding virtual terms their contribution to the cross section is expected to have a dependence on $W^2$ like in eq. (2.1), up to logarithmic corrections. They would contribute the $a_{02}$ coefficient in eq. (2.2).

## 3. The four-quark contribution to the $\mathcal{O}(\alpha_s^2)$ corrections

When calculating the four-quark contribution to $\gamma^*\gamma^* \to$ hadrons,

$$e^+e^- \to e^+e^-\gamma^*\gamma^* \to e^+e^- q\bar{q}Q\bar{Q}\,, \tag{3.1}$$

we assume that all the produced quarks are massless and that the virtualities $Q^2_{1,2}$ are low enough that contributions of virtual $W, Z$ bosons can be neglected. Indeed, for the four-quark contributions at 200 GeV centre-of-mass energy $\langle W\rangle \simeq 40\,\mathrm{GeV}$ and $\langle Q_i^2\rangle \simeq 13\,\mathrm{GeV}^2$. We have re-computed the tree amplitudes for four-quark production [30] using the spinor products of appendix A. The contributing diagrams are shown in figure 2, featuring gluon (figure 2$a$–$c$) or quark (figure 2$d$–$f$) exchange in the crossed channel. For two quark pairs of different flavour, we have

$$\mathcal{A}_8\left(1_q, 2_{\bar{q}}; 3_\ell, 4_{\bar{\ell}}, 5_{\bar{\ell}'}, 6_{\ell'}; 7_Q, 8_{\bar{Q}}\right) = 4e^4 g_S^2\, T^a_{i_1\bar{\imath}_2} T^a_{i_7\bar{\imath}_8}\, A_8(1,2;3,4,5,6;7,8)\,, \tag{3.2}$$

with $\{1,2\}$ and $\{7,8\}$ the quark pairs, and $\{3,4\}$ and $\{5,6\}$ the lepton pairs, and where the colour-stripped sub-amplitude $A_8$ depends on the momenta and helicities of the external particles. By convention, all particles are taken as outgoing, thus an incoming fermion of a given helicity is represented by an outgoing antifermion of the opposite helicity. $A_8$ can be divided into the functions $a_8$, $b_8$ and $c_8$,

$$\begin{aligned} A_8\left(1_q, 2_{\bar{q}}; 3_\ell, 4_{\bar{\ell}}, 5_{\bar{\ell}'}, 6_{\ell'}; 7_Q, 8_{\bar{Q}}\right) = \; & Q_{f_q} Q_{f_Q} a_8(1,2;3,4,5,6;7,8) + \\ & + Q^2_{f_q} b_8(1,2;3,4,5,6;7,8) + \\ & + Q^2_{f_Q} c_8(1,2;3,4,5,6;7,8)\,, \end{aligned} \tag{3.3}$$

with $Q_{f_{q(Q)}}$ the electric charge fraction of the quark $q(Q)$ of flavour $f_{q(Q)}$. The calculation of the functions $a_8$, $b_8$ and $c_8$ as well as the one of the related production rate is detailed in appendix B.

### 3.1 The high-energy limit

In section 2, we claimed that when the squared hadronic energy $W^2$ is much larger than the typical momentum transfer $\mu_W^2$, and radiative corrections to the gluon exchanged between two quark pairs are considered, the large logarithms of type $\ln(W^2/\mu_W^2)$ which ensue can be resummed through the BFKL ladder. In fact, the resummation of the BFKL ladder requires more restrictive kinematics, where the rapidities of quarks which do not belong to the same quark pair are strongly ordered,

$$\eta_1 \simeq \eta_2 \gg \eta_7 \simeq \eta_8 \qquad \mathit{or} \qquad \eta_1 \simeq \eta_2 \ll \eta_7 \simeq \eta_8 \,. \tag{3.4}$$

Equation (3.4) defines the *high-energy limit* for $\gamma^*\gamma^* \to$ hadrons. When the strong rapidity ordering (3.4) occurs, the diagrams with gluon exchange in the crossed channel yield the dominant contribution,[2] and in the amplitude (3.3) the functions $b_8$ and $c_8$ can be neglected. Thus the two final-state quark pairs can be treated as non-interacting, and in the squared amplitude we can take the quark flavours as always distinct,

$$\frac{1}{2}\sum_{f_q,f_Q} |A_8(1,2;3,4,5,6;7,8)|^2 = \frac{1}{2}\left(Q_u^2 n_u + Q_d^2 n_d\right)^2 |a_8(1,2;3,4,5,6;7,8)|^2 \,, \tag{3.5}$$

with $Q_u = 2/3$, $Q_d = -1/3$ and $n_{u(d)}$ the number of up(down)-type quarks. In eq. (3.5) the factor of 1/2 appears in order to avoid double counting, since the amplitudes are symmetric with respect to the interchange of the two quark lines. Thus for a fixed lepton-helicity configuration, e.g. $(3_\ell^-, 4_{\bar\ell}^+, 5_{\bar\ell'}^+, 6_{\ell'}^-)$, the production rate is

$$\begin{aligned}
d\sigma&\left(3_\ell^-, 4_{\bar\ell}^+, 5_{\bar\ell'}^+, 6_{\ell'}^-\right) = \\
&= \frac{1}{2s} d\mathcal{P}_6 16\left(N_c^2-1\right)(4\pi\alpha_{\mathrm{em}})^4(4\pi\alpha_S)^2 \frac{1}{2}\left(Q_u^2 n_u + Q_d^2 n_d\right)^2 \times \\
&\quad \times\Big[\left|a_8\left(1^-,2^+;3^-,4^+,5^+,6^-;7^-,8^+\right)\right|^2 + \left|a_8\left(2^-,1^+;3^-,4^+,5^+,6^-;7^-,8^+\right)\right|^2 + \\
&\qquad + \left|a_8\left(1^-,2^+;3^-,4^+,5^+,6^-;8^-,7^+\right)\right|^2 + \left|a_8\left(2^-,1^+;3^-,4^+,5^+,6^-;8^-,7^+\right)\right|^2\Big],
\end{aligned} \tag{3.6}$$

where the six-particle phase space is given in eq. (B.15). The other lepton-helicity configurations are simply obtained by exchanging the labels 3 and 4 and/or 5 and 6 in eq. (3.6) (see appendix B). The unpolarised rate is given by averaging over the rates for the four lepton-helicity configurations.

Since in the high-energy limit the two final-state quark pairs behave effectively as if they were two independent scattering centres, the amplitude (3.3) with the functions $b_8$ and $c_8$ set to zero is expected to factorise into two high-energy coefficient functions, usually termed impact factors, for the process $eg^* \to eq\bar{q}$, where $g^*$ is the off-shell gluon which is exchanged in the crossed channel. In the high-energy limit, the amplitude (3.3) can then be used to derive such impact factors. However, it is easier to invoke high-energy

[2] Note that the reverse is not true. In fact the diagrams with gluon exchange in the crossed channel may dominate over the diagrams with quark exchange well before the high-energy limit is realised. This issue is discussed in section 4.

JHEP05(2002)005

factorisation and to derive the impact factor for $eg^* \to eq\bar{q}$ from a simpler process, e.g. from the scattering amplitudes $eg \to q\bar{q}g$ or $eQ \to q\bar{q}Q$ which appear typically in DIS processes. Then one can use two such impact factors, one in the forward and one in the backward kinematics, connected by a gluon exchanged in the crossed channel, in order to obtain the amplitude for $e^+e^- \to q\bar{q}Q\bar{Q}$ in the high-energy limit. We denote the impact factor for the $eg^* \to eq\bar{q}$ process in the forward (backward) kinematics, evaluated in the $\gamma^*\gamma^*$ centre-of-mass frame, as $V_{f(b)}(p_{\bar{\ell}}; p_\ell, p_q, p_{\bar{q}})$ (remember that all momenta are outgoing, hence the dependence on momenta of two particles and two antiparticles), and derive it in appendix C (see eq. (C.16)). Then the amplitude (3.2) factorises as

$$\begin{aligned}
&\mathcal{A}_8\left(1_q, 2_{\bar{q}}; 3_\ell, 4_{\bar{\ell}}, 5_{\bar{\ell}'}, 6_{\ell'}; 7_Q, 8_{\bar{Q}}\right) = \\
&\quad = 2s_{\gamma^*\gamma^*}\left[g_S e^2 Q_{f_q}\, T^c_{i_1\bar{\imath}_2}\, \sqrt{2} V_f\left(4_{\bar{\ell}}; 3_\ell, 1_q, 2_{\bar{q}}\right)\right] \frac{1}{t} \left[g_S e^2 Q_{f_Q}\, T^c_{i_7\bar{\imath}_8}\, \sqrt{2} V_b\left(6_{\ell'}; 5_{\bar{\ell}'}, 7_Q, 8_{\bar{Q}}\right)\right],
\end{aligned} \tag{3.7}$$

with $t = q^2$, where $q = -\sum_{i=1}^4 p_i$ is the momentum transfer. The two impact factors for $eg^* \to eq\bar{q}$ can be extracted through re-labelling from eqs. (C.16)-(C.19). Each of those impact factors can be decomposed further into a lepton current and an impact factor for $\gamma^* g^* \to q\bar{q}$ (see eqs. (C.20)-(C.22)).

In computing the square of the amplitude, we must sum over helicity, colour and flavour of the quarks, however in this case the flavour sum is trivial since the two impact factors do not interfere and we can treat the quark flavours as always distinct. The production rate is

$$\begin{aligned}
d\sigma\left(3^-_\ell, 4^+_{\bar{\ell}}, 5^+_{\bar{\ell}'}, 6^-_{\ell'}\right) &= \frac{1}{2s} d\mathcal{P}_6\, 16\left(N_c^2 - 1\right)(4\pi\alpha_{\rm em})^4 (4\pi\alpha_S)^2 \left(Q_u^2 n_u + Q_d^2 n_d\right)^2 \times \\
&\times \frac{s^2_{\gamma^*\gamma^*}}{t^2}\left[\left(\left|V_f\left(4^+_{\bar{\ell}}; 3^-_\ell, 1^-_q, 2^+_{\bar{q}}\right)\right|^2 + \left|V_f\left(4^+_{\bar{\ell}}; 3^-_\ell, 1^+_q, 2^-_{\bar{q}}\right)\right|^2\right) \times \right. \\
&\left. \times \left(\left|V_b\left(5^+_{\bar{\ell}'}; 6^-_{\ell'}, 7^-_Q, 8^+_{\bar{Q}}\right)\right|^2 + \left|V_b\left(5^+_{\bar{\ell}'}; 6^-_{\ell'}, 7^+_Q, 8^-_{\bar{Q}}\right)\right|^2\right)\right],
\end{aligned} \tag{3.8}$$

which constitutes the high-energy factorisation of eq. (3.6). Each of the two rapidity orderings of eq. (3.4) yield the same contribution to eq. (3.8). Thus we have included them by taking only the first of the two and deleting the double counting factor 1/2. As in ref. [29, section 2.3], the phase space (B.15) for the $e^+e^- q\bar{q}Q\bar{Q}$ final state can be factorised into hadronic and leptonic phase spaces,

$$d\mathcal{P}_6 = d\Gamma(p_3, p_5)\, d\mathcal{P}_4(p_1, p_2, p_7, p_8; k_1 + k_2)\,, \tag{3.9}$$

with $k_1 = p_4 - p_3$ and $k_2 = p_6 - p_5$ the momenta of the virtual photons (here we have inverted the direction of $p_4$ and $p_6$ in order to have them incoming), and

$$\begin{aligned}
d\Gamma &= \frac{d^3p_3}{(2\pi)^3 2p_3^0}\frac{d^3p_5}{(2\pi)^3 2p_5^0} \\
d\mathcal{P}_4 &= \prod_{i=1,2,7,8} \frac{d^3p_i}{(2\pi)^3 2p_i^0}\, (2\pi)^4\, \delta^4(k_1 + k_2 - p_1 - p_2 - p_7 - p_8)\,,
\end{aligned} \tag{3.10}$$

the leptonic and hadronic phase spaces, respectively.

In the high-energy limit, momentum conservation for $e^+e^- \to e^+e^-\gamma^*\gamma^* \to e^+e^- q\bar{q}Q\bar{Q}$ implies that, in the $\gamma^*\gamma^*$ centre-of-mass frame,[3]

$$\begin{aligned} k_1^+ &\simeq p_1^+ + p_2^+ \\ k_2^- &\simeq p_7^- + p_8^- \\ 0 &= p_{1\perp} + p_{2\perp} + p_{7\perp} + p_{8\perp} \end{aligned} \tag{3.11}$$

where we use light-cone coordinates: $p^\pm = p^0 \pm p^z$ and for the two-dimensional vector $p_\perp$ complex transverse coordinates $p_\perp = p^x + ip^y$ (see appendix C). Momentum conservation (3.11) allows us to factorise the hadronic phase space (3.10) further,

$$\begin{aligned} \mathrm{d}\mathcal{P}_4 = 2 &\left( \prod_{i=1,2} \frac{d^3 p_i}{(2\pi)^3 2p_i^0}\, 2\pi\, \delta\left(k_1^+ - p_1^+ - p_2^+\right)\right) \left( \prod_{i=7,8} \frac{d^3 p_i}{(2\pi)^3 2p_i^0}\, 2\pi\, \delta\left(k_2^- - p_7^- - p_8^-\right)\right) \times \\ &\times (2\pi)^2\, \delta^2(p_{1\perp} + p_{2\perp} + p_{7\perp} + p_{8\perp})\,. \end{aligned} \tag{3.12}$$

The terms in round brackets in the first line are the phase spaces for the two impact factors. They are connected by transverse momentum conservation only. The overall factor of 2 in $\mathrm{d}\mathcal{P}_4$ comes from the jacobian of the light-cone coordinates. Equation (3.12) can be immediately generalised to the emission of a BFKL gluon ladder between the impact factors.

Fixing

$$x_a = \frac{p_1^+}{p_1^+ + p_2^+} = 1 - \tilde{x}_a\,, \qquad x_b = \frac{p_7^-}{p_7^- + p_8^-} = 1 - \tilde{x}_b\,, \tag{3.13}$$

the phase space (3.12) can be re-written as

$$\begin{aligned} \mathrm{d}\mathcal{P}_4 = &\frac{1}{(4\pi)^2} \frac{1}{2k_1^+ k_2^-} \left( \frac{dx_a}{x_a(1-x_a)} \frac{d^2 p_{1\perp}}{(2\pi)^2}\right) \left( \frac{dx_b}{x_b(1-x_b)} \frac{d^2 p_{7\perp}}{(2\pi)^2}\right) \times \\ &\times \frac{d^2 q_{a\perp}}{(2\pi)^2} \frac{d^2 q_{b\perp}}{(2\pi)^2} (2\pi)^2\, \delta^2(q_{a\perp} - q_{b\perp}) \end{aligned} \tag{3.14}$$

with $q_a = k_1 - p_1 - p_2$ and $q_b = p_7 + p_8 - k_2$. Note that in the $\gamma^*\gamma^*$ centre-of-mass frame, the momenta of the virtual photons are (in the light-cone notation of appendix C) $k_1 = (k_1^+, k_1^-; 0_\perp)$ and $k_2 = (k_2^+, k_2^-; 0_\perp)$, with virtualities $k_1^2 = k_1^+ k_1^- = -Q_1^2$ and $k_2^2 = k_2^+ k_2^- = -Q_2^2$. In the high-energy limit, $k_1^+ \gg k_1^-$ and $k_2^- \gg k_2^+$, thus the centre-of-mass energy is $s_{\gamma^*\gamma^*} = (k_1 + k_2)^2 \approx k_1^+ k_2^-$.

## 4. Theoretical predictions

In this section we present the results obtained by considering the contribution of the four parton final state to the cross section for $\gamma^*\gamma^* \to$ hadrons. The four parton final state is

[3]Equation (3.11) is valid also in $e^+e^-$ centre-of-mass frame by adding $p_{3\perp} + p_{5\perp}$ to the right hand side of the third line.

$\mathcal{O}(\alpha_{\rm em}^4\alpha_S^2)$, however from the stand point of both the electromagnetic and the strong corrections it is a leading order calculation, thus the dependence of either the electromagnetic or the strong coupling on the respective scales is maximal.

As far as $\alpha_{\rm em}$ is concerned, we have chosen to set the scales on an event-by-event basis to the virtualities of the exchanged photons; hence, we replace the Thomson value $\alpha_0 \simeq 1/137$ by $\alpha_{\rm em}(Q_i^2)$, as in ref. [29]. This choice better describes the effective strength at which the electromagnetic interaction takes place. In addition, we treat independently the two photon legs: thus, in the formulæ relevant to the cross sections, $\alpha_{\rm em}^4$ has to be understood as $\alpha_{\rm em}^2(Q_1^2)\alpha_{\rm em}^2(Q_2^2)$.

As far as $\alpha_S$ is concerned, we define a default scale $\mu_0$ so as to match the order of magnitude of the inverse of the interaction range [29],

$$\mu_0^2 = \frac{Q_1^2+Q_2^2}{2} + \left(\frac{p_{1\perp}+p_{2\perp}+p_{7\perp}+p_{8\perp}}{2}\right)^2 . \tag{4.1}$$

Scale choices other than (4.1) have been considered in ref. [29]. The renormalisation scale $\mu$ entering $\alpha_S$ is set equal to $\mu_0$ as a default value, and equal to $\mu_0/2$ or $2\mu_0$ when studying the scale dependence of the cross section. In eq. (4.1), the $p_{i\perp}$ are the transverse energies of the outgoing partons. Since the hard process is initiated by the two virtual photons, the proper frame to study its properties is the $\gamma^*\gamma^*$ centre-of-mass one. Therefore, when talking about transverse energies, whether in a total or in a jet cross section, this frame will be always understood.

We evolve $\alpha_S$ to next-to-leading log accuracy, with $\alpha_S(M_Z) = 0.1181$ [32] (in $\overline{\rm MS}$ at two loops and with five flavours, this implies $\Lambda^{(5)}_{\overline{\rm MS}} = 0.2275\,{\rm GeV}$). The choice of the two-loop running is due to the fact that we are going to use a full NLO calculation augmented by a partial $\mathcal{O}(\alpha_S^2)$ contribution (the diagrams of the $g$ class only). When presenting numerical results we use five massless flavours in the cross section formulae (3.8) and (B.9).

In exploring the footprints of the BFKL resummation in $e^+e^-$ collisions, it is customary to introduce the variable $Y$,

$$Y = \log \frac{y_1 y_2 s}{\sqrt{Q_1^2 Q_2^2}} , \tag{4.2}$$

where the variables $y_i$ are proportional to the light-cone momentum fraction of the virtual photons,

$$y_i = \frac{q_i^0 + q_i^3}{\sqrt{s}} = 1 - \frac{2E_i}{\sqrt{s}} \cos^2\frac{\theta_i}{2} , \qquad i = 1,2 , \tag{4.3}$$

where $E_i$ and $\theta_i$ are the energies and scattering angles of the outgoing electron and positron in the $e^+e^-$ centre-of-mass frame. For large $Y$, we have $y_1 y_2 s \approx W^2$, i.e. the $Y$ variable parametrises the ratio of the hadronic energy over a typical momentum transfer, thus it is a variable which is suitable for analyses of the BFKL type.

In figure 3, we plot the $Y$ distribution for different production rates. Namely, for the total NLO cross section (dot-long-dashed line), for the total cross section due to diagrams of the $g$ class only (solid line), for the four-jet cross section at $y_{\rm cut} = 0.01$ or $0.001$ (dot-short-dashed line) and for the four-jet cross section with diagrams of the $g$ class only at $y_{\rm cut} = 0.01$ (dashed line) and at $y_{\rm cut} = 0.001$ (dotted line). Throughout this plot and

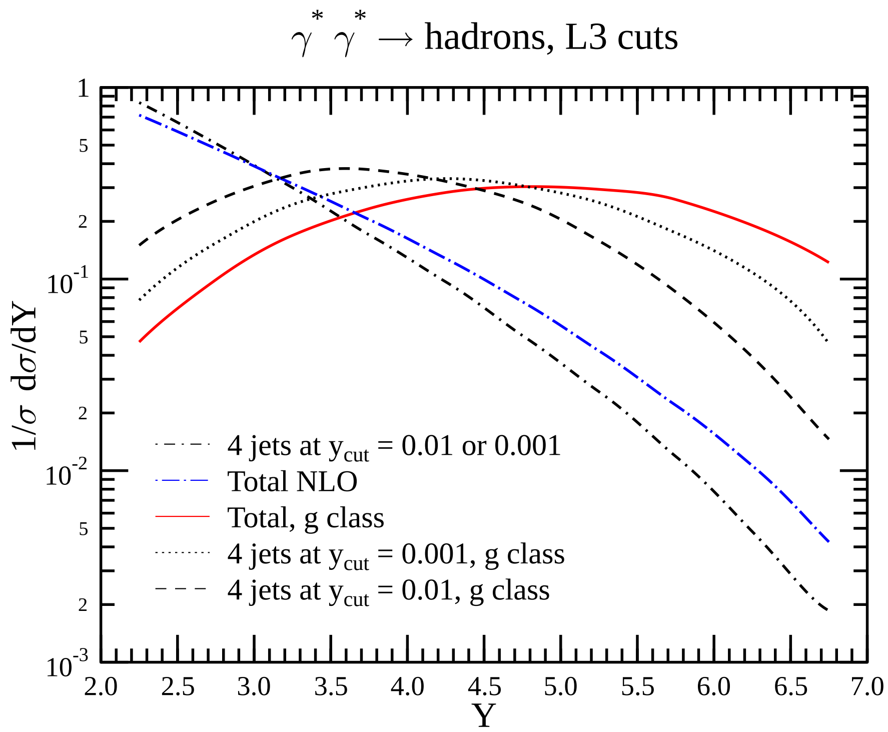


**Figure 3:** $Y$ distribution in different production rates. Namely, in the total NLO cross section (dot-long-dashed line), in the total cross section due to diagrams of the $g$ class only (solid line), in the four-jet cross section (dot-short-dashed line) and in the four-jet cross section with diagrams of the $g$ class only at $y_{\mathrm{cut}} = 0.01$ (dashed line) and at $y_{\mathrm{cut}} = 0.001$ (dotted line). The relative normalisation of the curves has been rescaled, in such a way that the area under each of the curves is the same.

henceforth, we use the acceptance cuts of the CERN L3 Collaboration [22], namely, the lepton energies $E_i$ are larger than 40 GeV, the lepton tagging angles $\theta_i$ are between 30 and 66 mrad and the hadronic energy $W$ is larger than 5 GeV. As far as the photon virtualities are concerned, the cuts above imply that $Q^2_{1,2} \gtrsim 4\,\mathrm{GeV}^2$. For the cross section due to diagrams of the $g$ class only, we use eq. (3.6). For the four-jet cross section, the four quark final states have been computed through the formulæ of appendix B; the final states with two quarks and two gluons have been generated with the help of MADGRAPH [33], which has been used also to check numerically the four-quark amplitudes of appendix B. In the jet cross sections, we define the jets through a $k_T$ algorithm [31]. The jet size is set by the $y_{\mathrm{cut}}$ variable. In figure 3 and 4 the normalisation of the curves is not relevant, since the contribution of the diagrams of the $f$ class to the total cross section cannot be inferred from the four-jet cross section, due to the lack of virtual corrections. Thus the relative normalisation of the curves has been rescaled, in such a way that the area under each of the curves is the same. Note that in figure 3 the shape of the four-jet cross section (dot-short-dashed line) is largely independent of the chosen $y_{\mathrm{cut}}$. In fact, there is basically no difference between the dot-short-dashed line at $y_{\mathrm{cut}} = 0.01$ or 0.001. At large $Y$ the four-jet cross section has a similar shape as the total NLO cross section (dot-long-dashed line). On

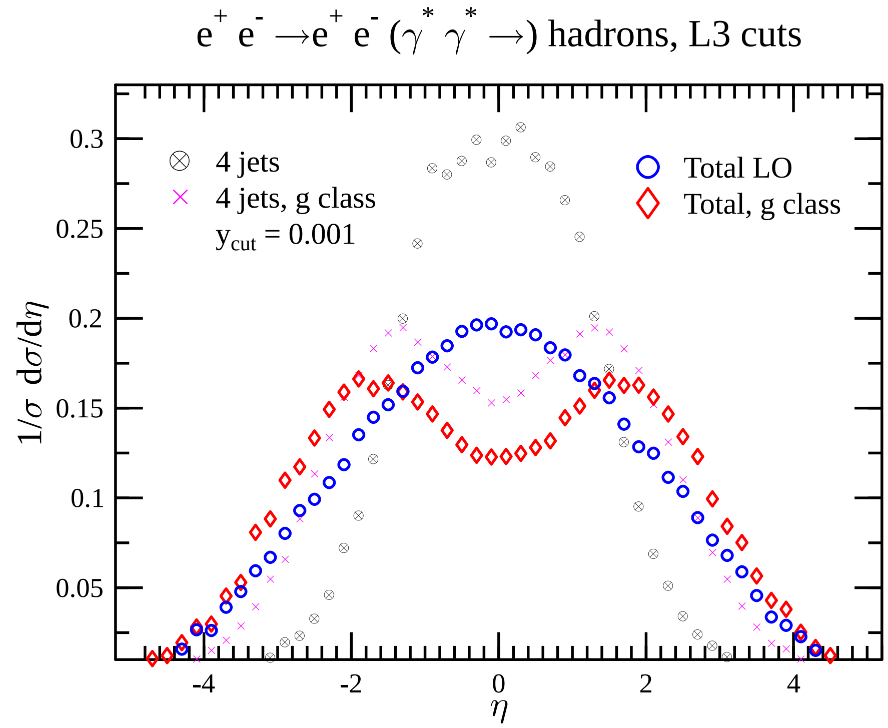


**Figure 4:** Rapidity distribution of one of the final-state partons, in different production rates. Namely, in the total LO cross section (*circles*), in the total cross section due to diagrams of the $g$ class only (*diamonds*), in the four-jet cross section (*circles with crosses*) and in the four-jet cross section with diagrams of the $g$ class only (*crosses*).

the contrary, at large $Y$ the four-jet cross section with diagrams of the $g$ class only gets a larger and larger contribution as $y_{\rm cut}$ goes from 0.01 (dashed line) to 0.001 (dotted line). In addition, the diagrams of the $g$ class are by themselves infrared finite. Thus in the four-jet cross section from diagrams of the $g$ class only, we can take the limit $y_{\rm cut} \to 0$ and obtain the total cross section (solid line). This has the most open shape at large $Y$, which hints that at large $Y$ we should expect a substantial contribution from the diagrams of the $g$ class to the total cross section at $\mathcal{O}(\alpha_S^2)$. The interference terms between the diagrams of the $g$ class and those of the $f$ class, i.e. the terms $2[Q_{f_q}^3 Q_{f_Q} \mathrm{Re}(a_8^* b_8) + Q_{f_q} Q_{f_Q}^3 \mathrm{Re}(a_8^* c_8)]$ in eq. (B.9), give also a finite contribution to the total cross section. We have checked that they yield a curve that is similar in shape to the total NLO cross section. Compared to the diagrams of the $g$ class (solid line), they yield an increase of at most 10 % only in the small-$Y$ region, their contribution being negligible at large $Y$. Thus we shall neglect them henceforth.

In figure 4, we plot the rapidity distribution of one of the final-state partons, in different production rates. Namely, in the total LO cross section (*circles*), in the total cross section due to diagrams of the $g$ class only (*diamonds*), in the four-jet cross section (*circles with crosses*) and in the four-jet cross section with diagrams of the $g$ class only (*crosses*). Note that, as expected, in the total LO cross section [29], which features two final-state partons with quark exchange in the crossed channel, the partons produced populate mainly the central rapidity region (*circles*). That is true also for the four-jet cross section (*circles with crosses*). Instead, in the four-jet cross section from diagrams of the $g$ class only (*crosses*), at $y_{\rm cut} = 0.001$, the produced quarks populate mainly the forward and backward rapidity regions. However, the shape of the *circles with crosses* curve depends on $y_{\rm cut}$ very mildly, while that of the *crosses* curve depends strongly on the chosen $y_{\rm cut}$. To understand how the latter comes about, we recall that the diagrams of the $g$ class feature two quark pairs separated by a gluon exchanged in the crossed channel, and therefore susceptible of being produced at large rapidity. In fact, the probability of finding one of them in the forward and backward rapidity regions grows as $y_{\rm cut}$ becomes smaller. In the limit $y_{\rm cut} \to 0$ we obtain the total cross section from diagrams of the $g$ class only (*diamonds*). That shows that it is more likely to produce the quarks in the forward and backward rapidity regions than it is to produce them in the central region.[4] Finally, we recall that in a full $\mathcal{O}(\alpha_S^2)$ calculation of the total cross section, at present unfeasible, the diagrams of the $f$ class are expected to yield a small correction to the NLO total cross section. Thus in a full NNLO calculation of the total cross section in the large $Y$ region, we expect the rapidity distribution of one of the final-state partons to be roughly a combination of the *circles* and *diamonds* curves.

Figures 3 and 4 show that in the large $Y$ region, the diagrams of the $g$ class yield an important contribution to the total cross section. Then it is natural to ask if, within the acceptance cuts of the LEP2 Collaborations, the hadronic energy $W$ is sufficiently high to warrant the use of the high-energy limit (3.4). We can answer that by comparing the exact contribution of the diagrams of the $g$ class (3.6) to the high-energy limit of the squared matrix element integrated over the exact phase space (3.8). That comparison is shown in figure 5, where the solid line is the contribution of the diagrams of the $g$ class and the dotted line is the high-energy limit of the squared matrix element. In this and in the following plots, the high-energy limit is obtained in the $\gamma^*\gamma^*$ centre-of-mass frame. In order to match the experimental accuracy, in the theoretical prediction we consider the high-energy limit as accurate only if the difference between the exact calculation and the high-energy limit is less than 20 %, which is a conservative upper limit of the total experimental error in the tail of the distributions (see the last bins in table 1). In figure 5 we see that their difference is less than 20 % only for $Y \gtrsim 7$. Unfortunately, the region where $Y \gtrsim 7$ is negligible at the LEP2 experiments, for the kinematic limit of $Y \approx 8$ is almost reached, thus the statistics are very small. We can collect the events in the high-energy region by separating the forward and backward rapidity regions, which can be achieved by requiring that the sum of the rapidities of the two most forward momenta, $\eta_f$, be larger than 3 and that of the other two (backward) momenta, $\eta_b$, be less than $-3$. The corresponding cross sections are also shown in figure 5 for the diagrams of the $g$ class (dashed line) and for the high-energy limit of the squared matrix element (dot-dashed line). These curves almost coincide with the cross sections without the rapidity separation for $Y \gtrsim 7$, but are distinctively smaller for $Y \lesssim 7$. This is consistent with the difference between the solid

[4]The position of the peaks as well as the depletion in the central rapidity region depends also on the cut on $Y$, e.g., if we use the cut $Y \geq 5$, the peaks move to about $\pm 3$ and become more pronounced.

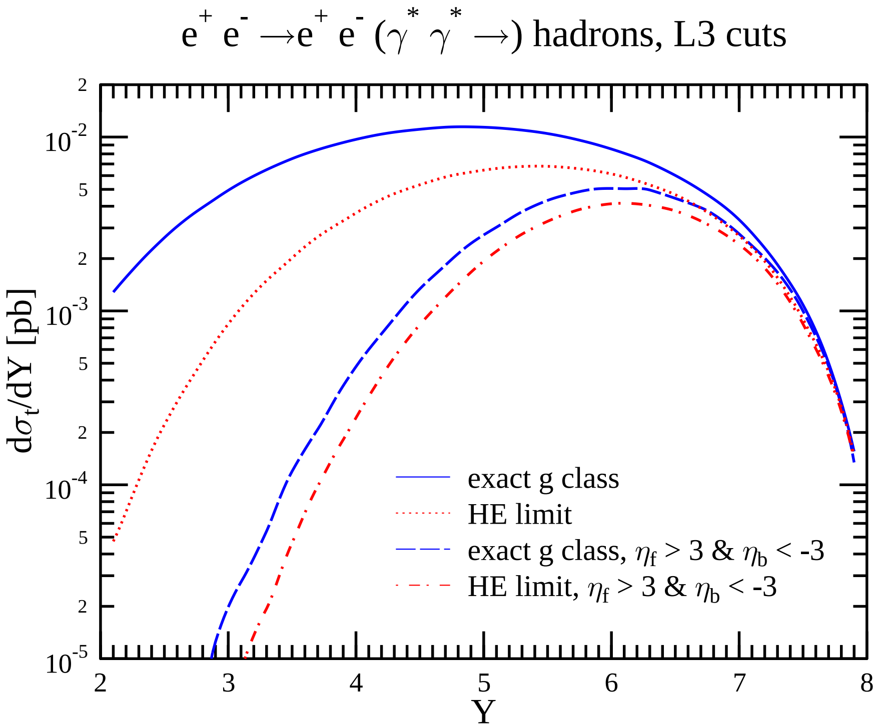


**Figure 5:** The total cross section as a function of $Y$. The solid (dashed) line represents the contribution of the diagrams of the $g$ class (with a rapidity cut), the dotted (dot-dashed) line represents the high-energy limit of the squared matrix element (with a rapidity cut).

and the dotted lines above. In addition, it shows that for a realistic set-up, i.e. for the cuts of the L3 Collaboration, the high-energy limit (3.4) is more stringent than the limit $W^2 \gg \mu_W^2$, the difference between the two being numerically negligible only for $Y \gtrsim 7$. Since the high-energy limit (3.4) is the kinematic framework of the BFKL resummation, we conclude that if a BFKL resummation is used in the $Y \lesssim 7$ region, we expect the subleading logarithmic corrections to be sizeable.

In figure 6, we plot the cross section as a function of the hadronic energy $W$ using different approximations: the solid line is the contribution of the diagrams of the $g$ class (3.6), the dashed line and the dot-dashed line are the high-energy limit of the squared matrix element integrated over the exact phase space (3.8) and the high-energy phase space (3.14), respectively. In the last one, the limit $s_{\gamma^*\gamma^*} \to \infty$ is taken and the transverse momenta of the quarks are integrated out analytically. Thus we shall term it the *analytic* high-energy limit. However, in this case we cannot use a renormalisation scale like eq. (4.1), which is defined on an event-by-event basis. Thus, for the sake of comparison, each cross section in figure 6 was obtained using the scale

$$\mu_0^2 = \frac{Q_1^2 + Q_2^2}{2}\,. \tag{4.4}$$

The three curves converge only for $W \gtrsim 100\,\text{GeV}$, which is again negligible at LEP2 for the poor statistics of the data. In addition, we see that for $W \lesssim 100\,\text{GeV}$ the analytic high-

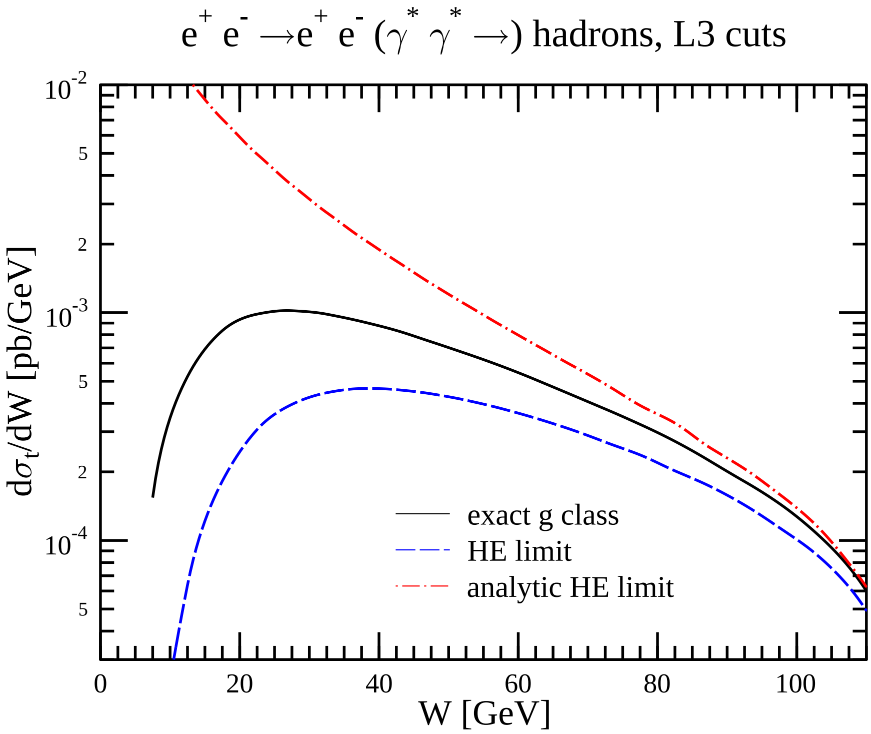


**Figure 6:** The total cross section as a function of the total hadronic energy $W$. The solid line is the contribution of the diagrams of the $g$ class, the dashed line and the dot-dashed line are the high-energy limit of the squared matrix element integrated over the exact phase space and the high-energy phase space, respectively.

energy limit[5] (dot-dashed line) significantly overestimates the exact contribution of the diagrams of the $g$ class. For instance, in the [40, 100] GeV range, considered by the CERN L3 Collaboration [22] (see the next section), the analytic high-energy limit prediction is about 60 % larger than the exact four-quark prediction. In figure 7, we plot the cross section as a function of $Y$ using the same approximations as in figure 6. Also the conclusions are basically the same as for figure 6, namely the three curves converge only for $Y \gtrsim 7$, while for $Y < 6$ the analytic high-energy limit significantly overestimates the exact contribution of the diagrams of the $g$ class. Note that the solid and dashed lines of figure 7 are the same as the solid and dotted lines of figure 5, but for using the renormalisation scale (4.4) instead of (4.1). Figure 8 has the same content as figure 7, but it is for a $e^+e^-$ future linear collider running at $\sqrt{s} = 500\,\mathrm{GeV}$. For the sake of illustration, we have taken the following acceptance cuts: the lepton energies are larger than 40 GeV, the lepton tagging angles are between 20 and 70 mrad and the hadronic energy is larger than 20 GeV. On the photon virtualities, the cuts above imply that $Q^2_{1,2} \gtrsim 4\,\mathrm{GeV}^2$, while the average virtualities are $\langle Q^2_i \rangle \simeq 36\,\mathrm{GeV}^2$. About the three curves, the same conclusions as for figure 7 can be drawn. However, the much larger statistics (at the designed luminosity, $\mathcal{L} = 3.4 \cdot 10^{34}\,\mathrm{cm}^{-2}\,\mathrm{s}^{-1}$ [34],

[5]In evaluating the analytic high-energy limit, we used the equivalent photon approximation for the lepton current (C.21), as in ref. [25].

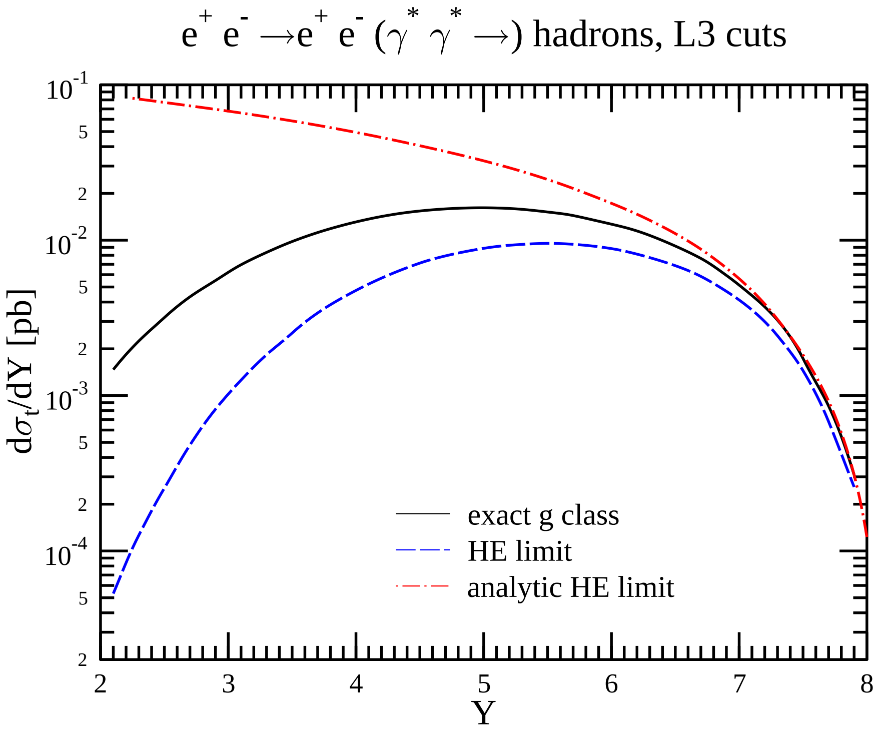


**Figure 7:** Same as figure 6, but with the total cross section as a function of $Y$.

we expect about 1700 events in ten days of continuous running) should make also the $Y \gtrsim 7$ region available to the analysis.

In conclusion, we have considered three successive approximations to the total cross section at $\mathcal{O}(\alpha_S^2)$:

- the contribution of the diagrams of the $g$ class only, eq. (3.6);
- the high-energy limit (3.4) of the squared matrix element, integrated over:
  - the exact phase space (3.8);
  - the high-energy phase space (3.14);

and we have seen that, although the contributions of the diagrams with gluon exchange in the crossed channel are numerically important in the high-$Y$ or high-$W$ regions, in the kinematic range of the LEP2 experiments the high-energy limit (3.4) is not sufficiently accurate.

## 5. Phenomenological results

In section 4, we have analysed the distributions in rapidity of the final-state partons, and their contribution to the total cross section in the large $Y$ or large $W$ regions. As expected, we have found that the diagrams of the $f$ class yield a contribution which in



JHEP05(2002)005

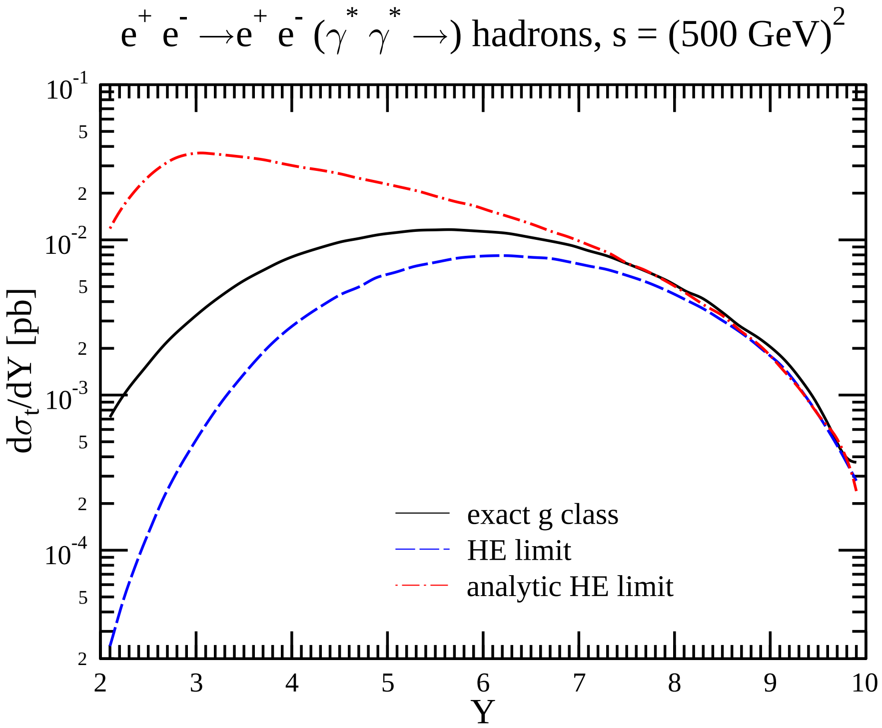


**Figure 8:** Same as figure 7, but for a future linear collider running at $\sqrt{s} = 500\,\mathrm{GeV}$.

shape is very similar to the one of the NLO calculation. Then we may argue that, if properly counterweighted by the virtual corrections, which at this moment are unknown, they would yield a rather minor numerical contribution, since they are an order in $\alpha_S$ higher than the NLO one. On the contrary, the diagrams of the $g$ class, which are by themselves finite and gauge invariant, have a very different shape in $Y$, becoming more and more numerically relevant as $Y$ grows. However, we have seen that in the kinematic range of the LEP2 experiments the diagrams of the $g$ class must be evaluated exactly, the high-energy limit (3.4) being not sufficiently accurate. Thus in this section we shall analyse the total cross section as a function of $Y$ through the NLO calculation and/or the diagrams of the $g$ class.

In figure 9, we plot the total cross section as a function of $Y$, at NLO (dot-dashed line) and at NLO plus the $\mathcal{O}(\alpha_S^2)$ contribution of the diagrams of the $g$ class (solid line). The shaded band has been obtained by varying the renormalisation scale from $\mu_0/2$ to $2mu_0$, with $mu_0$ given in (4.1). The points are the experimental data from the CERN L3 Collaboration [22]. The corresponding numbers are given in table 1. In computing the error bars, we added the statistical and systematic errors of the data in quadrature. We see that adding the diagrams of the $g$ class to the NLO calculation decreases the discrepancy between data and theory at large $Y$, however the data still lie above the theory prediction, even allowing for a scale uncertainty on the latter[6]. In addition, we remind that our

[6]We have also computed the total cross section as a function of $Y$, by using only the diagrams of the $g$

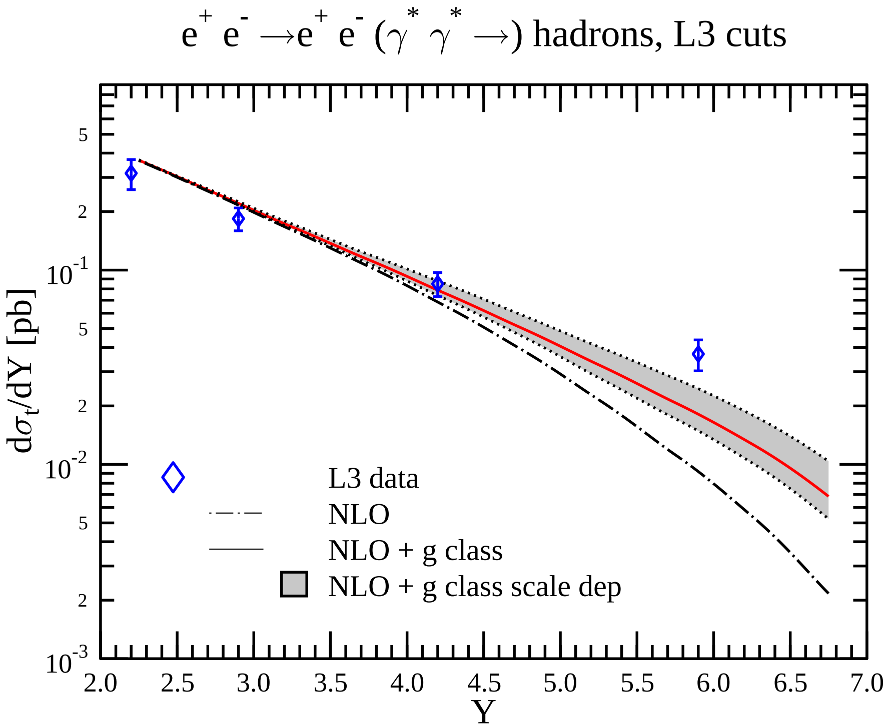


**Figure 9:** Total cross section as a function of $Y$, at NLO (dot-dashed line), and at NLO plus the $\mathcal{O}(\alpha_S^2)$ contribution of the diagrams of the $g$ class only (solid line). The shaded band has been obtained by varying the renormalisation scale from $\mu_0/2$ to $2\mu_0$. The points are the experimental data from the CERN L3 Collaboration [22]. In computing the error bars, we added their statistical and systematic errors in quadrature.

calculation is performed in the massless limit: no mass effect for final-state charm and bottom quarks have been included. In ref. [29] it was found the masses to decrease the LO cross section by 10–15%. A comparable depletion is expected at NLO. In the case of four quark production in the analytic high energy limit (defined in the discussion of figure 6), the masses were found to decrease the cross section by about 20% [27]. This correction should provide a lower bound to the exact mass correction in four quark production. Since the four quark contribution dominates over the NLO calculation at large $Y$, and is negligible at small $Y$, we should expect the inclusion of the mass corrections to decrease the solid line of figure 9 by about 10–15% at small $Y$ and by at least 20% at large $Y$. Therefore the inclusion of the mass dependence is expected to improve the agreement between data and theory at small $Y$ but to widen the discrepancy at large $Y$. The same considerations apply to figure 10, where the total cross section is plotted as a function of $W$. This was to be expected, since in the large $Y$ limit, $Y$ grows linearly with the logarithm of $W$.

class, i.e. without the NLO contribution, and evolving $\alpha_S$ with the one-loop running. For the high-$Y$ region ($Y \gtrsim 5$) the outcome is compatible in shape with the dot-dashed curve, thus it fails as well to describe the data.

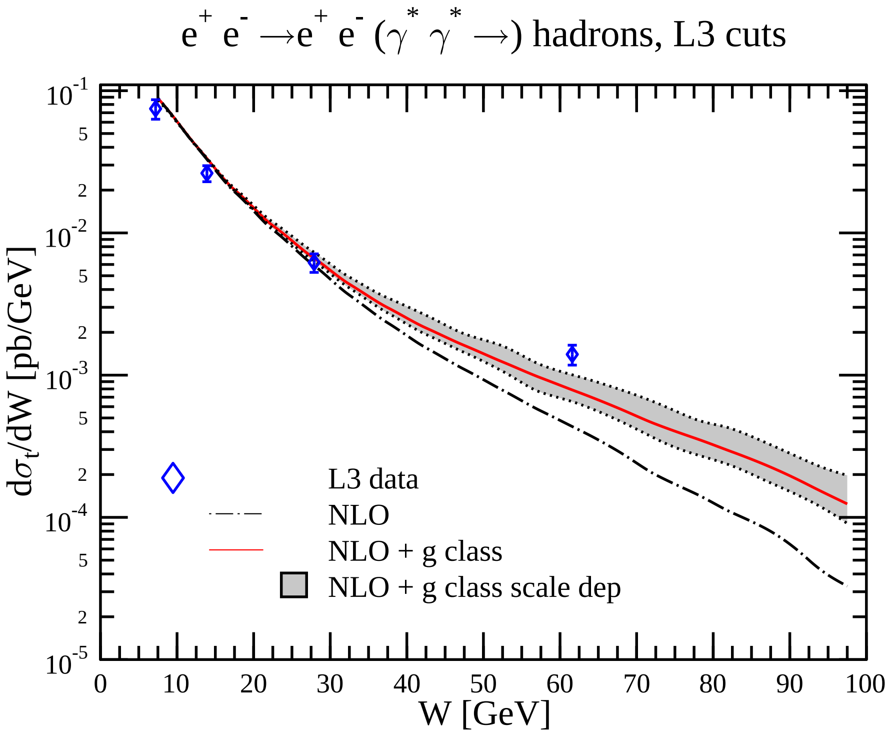


**Figure 10:** Same as in figure 9, but with the total cross section as a function of the hadronic energy $W$.

| $\Delta W$ (GeV) | L3 data $d\sigma_{ee}/dW$ (pb/GeV) | NLO $d\sigma_{ee}/dW$ (pb/GeV) | NLO + $g$ class $d\sigma_{ee}/dW$ (pb/GeV) |
|---|---|---|---|
| 5– 10 | $0.0747 \pm 0.0096 \pm 0.0067$ | $0.0883^{+0.0004}_{-0.0027}$ | $0.0885^{+0.0003}_{-0.0027}$ |
| 10– 20 | $0.0263 \pm 0.0024 \pm 0.0024$ | $0.0300^{+0.0001}_{-0.0001}$ | $0.0305^{+0.0003}_{-0.0002}$ |
| 20– 40 | $0.0062 \pm 0.0007 \pm 0.0006$ | $0.0057^{+0.0001}_{-0.0003}$ | $0.0064^{+0.0006}_{-0.0003}$ |
| 40–100 | $0.0014 \pm 0.0002 \pm 0.0001$ | $0.0004^{+0.0001}_{-0.0000}$ | $0.0007^{+0.0002}_{-0.0001}$ |
| $\Delta Y$ | L3 data $d\sigma_{ee}/dY$ (pb) | NLO $d\sigma_{ee}/dY$ (pb) | NLO + $g$ class $d\sigma_{ee}/dY$ (pb) |
| 2.0–2.5 | $0.315 \pm 0.048 \pm 0.028$ | $0.366^{+0.001}_{-0.001}$ | $0.368^{+0.002}_{-0.002}$ |
| 2.5–3.5 | $0.184 \pm 0.018 \pm 0.017$ | $0.203^{+0.002}_{-0.001}$ | $0.208^{+0.004}_{-0.003}$ |
| 3.5–5.0 | $0.085 \pm 0.009 \pm 0.008$ | $0.070^{+0.002}_{-0.002}$ | $0.080^{+0.008}_{-0.005}$ |
| 5.0–7.0 | $0.037 \pm 0.006 \pm 0.003$ | $0.010^{+0.001}_{-0.001}$ | $0.018^{+0.006}_{-0.003}$ |

**Table 1:** Differential cross sections in $W$ and $Y$ for the process $e^+e^- \to$ hadrons. For the data the first uncertainty is statistical and the second systematic. For the theoretical predictions the error is given by the renormalization-scale ambiguity.

## 6. Conclusions

In ref. [29], the question had been addressed of whether the LEP2 data for the total cross section of $\gamma^*\gamma^* \to$ hadrons could be described by a NLO calculation. It was found that the NLO analysis described well the data, except at the high end of the hadronic energy spectrum. Through the analysis of the inclusive jet and dijet cross sections, different kinematic regions were explored, and it was argued that the region of large $Y$ is particularly susceptible to large logarithms of type $\ln(W^2/\mu_W^2)$.

In this work, we have included in the analysis the four parton final states, which are part of the $\mathcal{O}(\alpha_S^2)$ contribution to the total cross section. The four–parton final states, which have been included in the massless limit, contain the diagrams with gluon exchange in the crossed channel, i.e. the diagrams of the $g$ class, which constitute the leading order of the BFKL resummation. In section 4, we have shown that indeed they play an important role in the large $Y$ region, however they must be evaluated *exactly*. In fact, the high-energy limit (3.4), which constitutes the kinematic framework of the BFKL resummation, is not sufficiently accurate at LEP2 energies, when compared to the experimental accuracy. Thus, if a BFKL resummation is used in the large $Y$ region, we expect the subleading logarithmic corrections to be sizeable.

In section 5, we have shown that the contribution of the diagrams of the $g$ class to the total cross section reduces the discrepancy between the theory and the LEP2 data of the L3 Collaboration. However, even allowing for the large scale uncertainty, which is intrinsic to the diagrams of the $g$ class since they appear for the first time at $\mathcal{O}(\alpha_S^2)$, the LEP2 data still lie above the theory. We remind the reader that in the NLO calculation and in the exact four–quark contribution quark mass effects have not been included. The inclusion of the mass dependence is expected to improve the agreement between data and theory at small $Y$ but to widen the discrepancy at large $Y$. Thus, in order to describe accurately the data for $\gamma^*\gamma^* \to$ hadrons, mass effects should be included, and eventually in the large $Y$ region corrections of an order higher than $\mathcal{O}(\alpha_S^2)$ should be considered.

## Acknowledgments

We should like to thank S. Catani, S. Frixione, F. Hautmann, W. Kilgore and M.L. Mangano for useful discussions. FM and ZT thank the INFN, sezione di Torino, for its kind hospitality during the late stage of this work. This work was supported in part by the EU Fourth Framework Programme "Training and Mobility of Researchers", Network "QCD and particle structure", contract FMRX-CT98-0194 (DG 12 - MIHT) and by the Hungarian Scientific Research Fund grants OTKA T-025482 and T-038240.

## A. Chiral-spinor algebra

In order to evaluate the production rates, we use helicity amplitudes, defined in terms of massless Dirac spinors $\psi_\pm(p)$ of fixed helicity,

$$\psi_\pm(p) = \frac{1 \pm \gamma_5}{2}\psi(p) \equiv |p^\pm\rangle \,, \qquad \overline{\psi_\pm(p)} \equiv \langle p^\pm| \,, \tag{A.1}$$

spinor products,

$$\langle pk\rangle \equiv \langle p^-|k^+\rangle \,, \qquad [pk] \equiv \langle p^+|k^-\rangle \,, \tag{A.2}$$

currents,

$$\begin{aligned} \langle i|k|j\rangle &\equiv \langle i^-|\not{k}|j^-\rangle = \langle ik\rangle\,[kj]\ , \\ \langle i|(k+l)|j\rangle &\equiv \langle i^-|(\not{k}+\not{l})|j^-\rangle \end{aligned} \tag{A.3}$$

and Mandelstam invariants

$$s_{pk} = 2p\cdot k = \langle pk\rangle\,[kp]\ , \qquad t_{pkq} = (p+k+q)^2\,, \qquad t_{pkql} = (p+k+q+l)^2\,. \tag{A.4}$$

## B. Four-quark production

The helicity amplitude featuring two quark pairs and two lepton pairs is

$$\mathcal{A}_8\left(1_q, 2_{\bar{q}}; 3_\ell, 4_{\bar{\ell}}, 5_{\bar{\ell}'}, 6_{\ell'}; 7_Q, 8_{\bar{Q}}\right) = 4e^4 g_S^2\, T^a_{i_1\bar{\imath}_2} T^a_{i_7\bar{\imath}_8}\ A_8(1,2;3,4,5,6;7,8)\,, \tag{B.1}$$

for two quark pairs of different flavour, and with $\{1,2\}$ and $\{7,8\}$ the quark pairs,[7] and $\{3,4\}$ and $\{5,6\}$ the lepton pairs. In the colour-stripped sub-amplitude $A_8$, the fermion flavours, momenta and helicities are implicit in the labels. $A_8$ is divided into the functions $a_8$, $b_8$ and $c_8$,

$$\begin{aligned} A_8\left(1_q, 2_{\bar{q}}; 3_\ell, 4_{\bar{\ell}}, 5_{\bar{\ell}'}, 6_{\ell'}; 7_Q, 8_{\bar{Q}}\right) = Q_{f_q} Q_{f_Q} a_8(1,2;3,4,5,6;7,8) + \\ + Q_{f_q}^2 b_8(1,2;3,4,5,6;7,8) + Q_{f_Q}^2 c_8(1,2;3,4,5,6;7,8)\,, \end{aligned} \tag{B.2}$$

with $Q_{f_{q(Q)}}$ the electric charge of the quark $q(Q)$ of flavour $f_{q(Q)}$ and

$$\begin{aligned} a_8(1,2;3,4,5,6;7,8) &= g_a(1,2;3,4,5,6;7,8) + g_a(1,2;6,5,4,3;7,8) + \\ &\quad + g_b(1,2;3,4,5,6;7,8) + g_c(1,2;3,4,5,6;7,8) + \\ &\quad + (\{1,2\} \leftrightarrow \{7,8\}) \\ b_8(1,2;3,4,5,6;7,8) &= f(1,2;3,4,5,6;7,8) + f(1,2;6,5,4,3;7,8) \\ c_8(1,2;3,4,5,6;7,8) &= b_8(7,8;3,4,5,6;1,2)\,, \end{aligned} \tag{B.3}$$

where in the quark pair exchange $(\{1,2\} \leftrightarrow \{7,8\})$ we swap the momentum and helicity labels of the (anti)quarks. In eq. (B.2) we have factored the flavour dependence in the quark electric charges, thus the functions $a_8$, $b_8$ and $c_8$ are independent of the quark flavours. In addition, because of the explicit sum in eq. (B.3) over the different orientations of the quark lines, the labels of the partons 1 and 7 refer only to quarks, and not to antiquarks. For distinct flavours each of the functions $a_8$, $b_8$ and $c_8$ is gauge invariant. The functions $g(f)$ refer to diagrams which feature gluon (quark) exchange in the crossed channel, figure 2. The functions $g_b$ and $g_c$ are symmetric under the exchange of the quark pairs and of the lepton pairs,

$$g_i(1,2;3,4,5,6;7,8) = g_i(7,8;6,5,4,3;1,2) \qquad i = b,c \tag{B.4}$$

[7]We normalise the colour matrices in the fundamental representation as $\mathrm{tr}(T^aT^b) = \delta^{ab}$.

For the configuration $(1^-, 2^+; 3^-, 4^+, 5^+, 6^-; 7^-, 8^+)$, the functions $g_a$, $g_b$, $g_c$ and $f$ are,

$$g_a = i\,\frac{\langle 1\,3\rangle\,[5\,8]\,\langle 6|(5+8)|2\rangle\langle 7|(1+3)|4\rangle}{s_{34}\,s_{56}\,t_{134}t_{568}t_{1234}} \tag{B.5}$$

$$g_b = i\,\frac{\langle 1\,3\rangle\,\langle 6\,7\rangle\,[2\,8]\,\left([5\,6]\,\langle 6|(1+3)|4\rangle + [5\,7]\,\langle 7|(1+3)|4\rangle\right)}{s_{34}\,s_{56}\,t_{134}\,t_{567}\,t_{1234}} \tag{B.6}$$

$$g_c = i\,\frac{\langle 1\,7\rangle\,[2\,4]\,[5\,8]\,\left(\langle 2\,3\rangle\,\langle 6|(5+8)|2\rangle + \langle 4\,3\rangle\,\langle 6|(5+8)|4\rangle\right)}{s_{34}\,s_{56}\,t_{234}\,t_{568}\,t_{1234}} \tag{B.7}$$

$$\begin{aligned} f = i\Bigg( &\frac{\langle 1\,3\rangle\,[2\,5]\,\langle 6|(2+5)|8\rangle\langle 7|(1+3)|4\rangle}{s_{34}\,s_{56}\,s_{78}\,t_{134}\,t_{256}} + \\ &+\frac{\langle 1\,7\rangle\,[2\,5]\,\langle 6|(2+5)|4\rangle\langle 3|(1+7)|8\rangle}{s_{34}\,s_{56}\,s_{78}\,t_{178}\,t_{256}} + \\ &+\frac{\langle 1\,3\rangle\,[2\,8]\,\langle 7|(2+8)|5\rangle\langle 6|(1+3)|4\rangle}{s_{34}\,s_{56}\,s_{78}\,t_{134}\,t_{278}}\Bigg). \end{aligned} \tag{B.8}$$

For all of the other helicity configurations, the functions $g_a$, $g_b$, $g_c$ and $f$ assume a functional form which is in principle different, however, the other lepton-helicity configurations are simply obtained by exchanging the labels 3 and 4 and/or 5 and 6 in eq. (B.1). Analogously, we show in appendix B.1 that the other quark-helicity configurations are obtained by exchanging the labels 1 and 2 and/or 7 and 8.

In the squared amplitude, the sum over distinct flavours can be written as

$$\begin{aligned} &\frac{1}{2}\sum_{f_q, f_Q \neq f_q} |A_8(1,2;3,4,5,6;7,8)|^2 = \\ &= \frac{1}{2}\Bigg[\sum_{f_q, f_Q \neq f_q}\Big\{Q_{f_q}^2 Q_{f_Q}^2\,\left[|a_8|^2 + 2\mathrm{Re}(b_8^* c_8)\right] + 2Q_{f_q}^3 Q_{f_Q}\mathrm{Re}(a_8^* b_8) + 2Q_{f_q} Q_{f_Q}^3\mathrm{Re}(a_8^* c_8)\Big\} + \\ &\quad + (n_f - 1)\Big(\sum_f Q_f^4\Big)\left(|b_8|^2 + |c_8|^2\right)\Bigg], \end{aligned} \tag{B.9}$$

with $n_f$ the number of quark flavours, and

$$\sum_f Q_f^4 = Q_u^4 n_u + Q_d^4 n_d \tag{B.10}$$

$$\sum_{f_q, f_Q \neq f_q} Q_{f_q}^i Q_{f_Q}^j = Q_u^i Q_u^j n_u(n_u - 1) + Q_d^i Q_d^j n_d(n_d - 1) + \left(Q_u^i Q_d^j + Q_u^j Q_d^i\right) n_u n_d$$

with $i, j$ any integer power, and with $Q_u = 2/3$, $Q_d = -1/3$ and $n_{u(d)}$ the number of up(down)-type quarks. In eq. (B.9) the factor of 1/2 appears in order to avoid double counting, since the amplitudes are symmetric with respect to the interchange of the two quark lines.

For two quark pairs of equal flavour, the sub-amplitude $A_8$ of eq. (B.2) becomes

$$A_8^{\mathrm{id}}\,(1_q, 2_{\bar{q}}; 3_\ell, 4_{\bar{\ell}}, 5_{\bar{\ell}'}, 6_{\ell'}; 7_q, 8_{\bar{q}}) = Q_f^2 a_8^{\mathrm{id}}(1,2;3,4,5,6;7,8)\,, \tag{B.11}$$

with

$$
\begin{aligned}
a_8^{\rm id}(1,2;3,4,5,6;7,8) \;=\;& g_a(1,2;3,4,5,6;7,8) + g_a(1,2;6,5,4,3;7,8) + \\
& + g_b(1,2;3,4,5,6;7,8) + g_c(1,2;3,4,5,6;7,8) + \\
& + f(1,2;3,4,5,6;7,8) + f(1,2;6,5,4,3;7,8) + \\
& + (\{1,2\} \leftrightarrow \{7,8\}) \,. \qquad \text{(B.12)}
\end{aligned}
$$

Note that in this instance the diagrams with gluon exchange in the crossed channel, corresponding to the functions $g_a$, $g_b$ and $g_c$, are in the same gauge class, while those featuring quark exchange in the crossed channel form a different gauge class. In addition, quarks of equal flavour are indistinguishable, thus we must add to eq. (B.1) the contribution with the quarks (but not the anti-quarks) exchanged, and antisymmetrise the whole amplitude in the colour and momentum labels,

$$
\begin{aligned}
&\mathcal{A}_8^{\rm id}(1_q,2_{\bar q};3_\ell,4_{\bar\ell},5_{\bar\ell'},6_{\ell'};7_q,8_{\bar q}) = 4e^4 g_S^2 \times \\
&\times\frac{1}{2}\Big\{ \left[(T^a)_{i_1\bar\imath_2}(T^a)_{i_7\bar\imath_8} + (T^a)_{i_7\bar\imath_2}(T^a)_{i_1\bar\imath_8}\right]\left[A_8^{\rm id}(1,2;3,4,5,6;7,8) - A_8^{\rm id}(7,2;3,4,5,6;1,8)\right] + \\
&\qquad + \left[(T^a)_{i_1\bar\imath_2}(T^a)_{i_7\bar\imath_8} - (T^a)_{i_7\bar\imath_2}(T^a)_{i_1\bar\imath_8}\right]\left[A_8^{\rm id}(1,2;3,4,5,6;7,8) + A_8^{\rm id}(7,2;3,4,5,6;1,8)\right]\Big\} \\
&= 4e^4 g_S^2\left[(T^a)_{i_1\bar\imath_2}(T^a)_{i_7\bar\imath_8} A_8^{\rm id}(1,2;3,4,5,6;7,8) - (T^a)_{i_7\bar\imath_2}(T^a)_{i_1\bar\imath_8} A_8^{\rm id}(7,2;3,4,5,6;1,8)\right] , \qquad \text{(B.13)}
\end{aligned}
$$

i.e. we can antisymmetrise eqs. (B.1) and (B.11) by subtracting the same expression with the colour and momentum labels of the quarks exchanged.

In crossing to the physical region, we choose 4 as the incoming electron and 6 as the incoming positron. For a fixed lepton-helicity configuration, e.g. $(3^-_\ell,4^+_{\bar\ell},5^+_{\bar\ell'},6^-_{\ell'})$, the production rate is obtained by summing over the quark-helicity configurations,

$$
\begin{aligned}
&d\sigma\left(3^-_\ell,4^+_{\bar\ell},5^+_{\bar\ell'},6^-_{\ell'}\right) = \frac{1}{2s} d\mathcal{P}_6 16\left(N_c^2-1\right)(4\pi\alpha_{\rm em})^4 (4\pi\alpha_S)^2 \times \qquad \text{(B.14)} \\
&\times\Bigg\{ \frac{1}{2}\sum_{f_q,f_Q\neq f_q}\Big[|A_8(1^-,2^+;3^-,4^+,5^+,6^-;7^-,8^+)|^2 + |A_8(2^-,1^+;3^-,4^+,5^+,6^-;7^-,8^+)|^2 + \\
&\qquad + |A_8(1^-,2^+;3^-,4^+,5^+,6^-;8^-,7^+)|^2 + |A_8(2^-,1^+;3^-,4^+,5^+,6^-;8^-,7^+)|^2\Big] + \\
&\quad + \frac{1}{4}\Big(\sum_f Q_f^4\Big)\Big[|a_8^{\rm id}(1^-,2^+;3^-,4^+,5^+,6^-;7^-,8^+)|^2 + |a_8^{\rm id}(7^-,2^+;3^-,4^+,5^+,6^-;1^-,8^+)|^2 + \\
&\qquad + \frac{2}{N_c}{\rm Re}\left[a_8^{\rm id}(1^-,2^+;3^-,4^+,5^+,6^-;7^-,8^+)^* a_8^{\rm id}(7^-,2^+;3^-,4^+,5^+,6^-;1^-,8^+)\right] + \\
&\qquad + |a_8^{\rm id}(2^-,1^+;3^-,4^+,5^+,6^-;7^-,8^+)|^2 + |a_8^{\rm id}(1^-,2^+;3^-,4^+,5^+,6^-;8^-,7^+)|^2 + \\
&\qquad + |a_8^{\rm id}(7^-,2^+;3^-,4^+,5^+,6^-;8^-,1^+)|^2 + |a_8^{\rm id}(2^-,7^+;3^-,4^+,5^+,6^-;1^-,8^+)|^2 + \\
&\qquad + |a_8^{\rm id}(2^-,1^+;3^-,4^+,5^+,6^-;8^-,7^+)|^2 + |a_8^{\rm id}(2^-,7^+;3^-,4^+,5^+,6^-;8^-,1^+)|^2 + \\
&\qquad + \frac{2}{N_c}{\rm Re}\left[a_8^{\rm id}(2^-,1^+;3^-,4^+,5^+,6^-;8^-,7^+)^* a_8^{\rm id}(2^-,7^+;3^-,4^+,5^+,6^-;8^-,1^+)\right]\Big]\Bigg\} ,
\end{aligned}
$$

where $d\mathcal{P}_6$ is the phase space for the $e^+e^- q\bar q Q\bar Q$ final state,

$$
d\mathcal{P}_6 = \prod_i \frac{d^3p_i}{(2\pi)^3 2E_i}\,(2\pi)^4\,\delta^4(p_4+p_6-p_1-p_2-p_3-p_5-p_7-p_8)\,, \qquad \text{(B.15)}
$$

with $i = 1, 2, 3, 5, 7, 8$. In eq. (B.14) we have performed explicitly the sum over quarks of equal flavour, and we have multiplied by the symmetry factor 1/4 for two identical quarks and two identical antiquarks. The sum over quarks of different flavour is performed in eq. (B.9). The unpolarised rate is given by averaging over the rates for the four lepton-helicity configurations.

### B.1 Symmetries under helicity flips of the quark lines

Symmetry relations between the functions $g_a$, $g_b$, $g_c$ and $f$ with respect to the configuration $(1^-,2^+;3^-,4^+,5^+,6^-;7^-,8^+)$,

(a) under helicity flip of the pair $\{1,2\}$,

$$\begin{aligned}
g_a(1^+,2^-;3^-,4^+,5^+,6^-;7^-,8^+) &= -g_c(2^-,1^+;3^-,4^+,5^+,6^-;7^-,8^+)\\
g_a(7^-,8^+;3^-,4^+,5^+,6^-;1^+,2^-) &= -g_b(2^-,1^+;6^-,5^+,4^+,3^-;7^-,8^+)\\
g_b(1^+,2^-;3^-,4^+,5^+,6^-;7^-,8^+) &= -g_a(7^-,8^+;6^-,5^+,4^+,3^-;2^-,1^+)\\
g_c(1^+,2^-;3^-,4^+,5^+,6^-;7^-,8^+) &= -g_a(2^-,1^+;3^-,4^+,5^+,6^-;7^-,8^+)\\
f(1^+,2^-;3^-,4^+,5^+,6^-;7^-,8^+) &= -f(2^-,1^+;6^-,5^+,4^+,3^-;7^-,8^+)\\
f(7^-,8^+;3^-,4^+,5^+,6^-;1^+,2^-) &= -f(7^-,8^+;3^-,4^+,5^+,6^-;2^-,1^+)
\end{aligned} \tag{B.16}$$

(b) under helicity flip of the pair $\{7,8\}$,

$$\begin{aligned}
g_a(1^-,2^+;3^-,4^+,5^+,6^-;7^+,8^-) &= -g_b(1^-,2^+;3^-,4^+,5^+,6^-;8^-,7^+)\\
g_a(7^+,8^-;3^-,4^+,5^+,6^-;1^-,2^+) &= -g_c(1^-,2^+;6^-,5^+,4^+,3^-;8^-,7^+)\\
g_b(1^-,2^+;3^-,4^+,5^+,6^-;7^+,8^-) &= -g_a(1^-,2^+;3^-,4^+,5^+,6^-;8^-,7^+)\\
g_c(1^-,2^+;3^-,4^+,5^+,6^-;7^+,8^-) &= -g_a(8^-,7^+;6^-,5^+,4^+,3^-;1^-,2^+)\\
f(1^-,2^+;3^-,4^+,5^+,6^-;7^+,8^-) &= -f(1^-,2^+;3^-,4^+,5^+,6^-;8^-,7^+)\\
f(7^+,8^-;3^-,4^+,5^+,6^-;1^-,2^+) &= -f(8^-,7^+;6^-,5^+,4^+,3^-;1^-,2^+)
\end{aligned} \tag{B.17}$$

(c) under helicity flips of the pairs $\{1,2\}$ and $\{7,8\}$, reflection

$$\begin{aligned}
g_a(1^+,2^-;3^-,4^+,5^+,6^-;7^+,8^-) &= g_a(8^-,7^+;6^-,5^+,4^+,3^-;2^-,1^+)\\
g_a(7^+,8^-;3^-,4^+,5^+,6^-;1^+,2^-) &= g_a(2^-,1^+;6^-,5^+,4^+,3^-;8^-,7^+)\\
g_b(1^+,2^-;3^-,4^+,5^+,6^-;7^+,8^-) &= g_c(2^-,1^+;3^-,4^+,5^+,6^-;8^-,7^+)\\
g_c(1^+,2^-;3^-,4^+,5^+,6^-;7^+,8^-) &= g_b(2^-,1^+;3^-,4^+,5^+,6^-;8^-,7^+)\\
f(1^+,2^-;3^-,4^+,5^+,6^-;7^+,8^-) &= f(2^-,1^+;6^-,5^+,4^+,3^-;8^-,7^+)\\
f(7^+,8^-;3^-,4^+,5^+,6^-;1^+,2^-) &= f(8^-,7^+;6^-,5^+,4^+,3^-;2^-,1^+)
\end{aligned} \tag{B.18}$$

Equations (B.16)–(B.18) show that the helicity flip of the pairs $\{1,2\}$ and/or $\{7,8\}$ reshuffles the functions in eq. (3.3) however it does not change their sum but only the overall sign, thus the helicity flip of the pairs $\{1,2\}$ and/or $\{7,8\}$ of the sub-amplitude (3.3) can be achieved by merely exchanging the corresponding labels.



JHEP05(2002)005

## C. The impact factor for $\gamma^* g^* \to q\bar{q}$

In order to derive the impact factor for $\gamma^* g^* \to q\bar{q}$, the simplest is to use either the amplitudes for $e^+e^- \to q\bar{q}gg$ or those for $e^+e^- \to q\bar{q}Q\bar{Q}$. They are collected, for instance, in ref. [35]. We shall take a lepton and a parton (quark or gluon), of momenta $p_a$ and $p_b$ respectively as the incoming particles, and a lepton, a quark pair and a parton of momenta $p_{a'}$, $p_1$, $p_2$ and $p_{b'}$ as the outgoing particles. All momenta are taken as outgoing, so that momentum conservation reads $p_a+p_b+p_{a'}+p_1+p_2+p_{b'} = 0$. We use light-cone coordinates: $p^\pm = p^0 \pm p^z$ and complex transverse coordinates $p_\perp = p^x + ip^y$, and write a four vector $p^\mu = (p^0, p^1, p^2, p^3)$ as $(p^+, p^-; p_\perp, \bar{p}_\perp)$, where $\bar{p}_\perp = p^x - ip^y$. With this notation the scalar product is $2p \cdot q = p^+q^- + p^-q^+ - p_\perp\bar{q}_\perp - \bar{p}_\perp q_\perp$. For real four vectors, e.g. for momenta, for which $\bar{p}_\perp = p^*_\perp$, we shall use the shorter notation $p = (p^+, p^-; p_\perp)$.

We define the photon momentum to be $k = -p_a - p_{a'}$, and choose as the reference frame the virtual photon-parton frame, defined by $p_b = (0, p_b^-; 0_\perp)$ and $k = (k^+, k^-; 0_\perp)$. Momentum conservation requires that

$$\begin{aligned} k^+ &= p_1^+ + p_2^+ + p_{b'}^+ \\ k^- &= p_1^- + p_2^- + p_b^- + p_{b'}^- \\ 0 &= p_{1\perp} + p_{2\perp} + p_{b'\perp} \end{aligned} \tag{C.1}$$

Now we take the high-energy limit, where the outgoing partons are strongly ordered on the light cone and have comparable transverse momentum,

$$p_1^+ \simeq p_2^+ \gg p_{b'}^+ ; \qquad p_1^- \simeq p_2^- \ll p_{b'}^- ; \qquad |p_{1\perp}| \simeq |p_{2\perp}| \simeq |p_{b'\perp}| . \tag{C.2}$$

While the transverse components of eq. (C.1) remain untouched, the light-cone components are approximated by $k^+ \simeq p_1^+ + p_2^+$ and $k^- \simeq p_b^- + p_{b'}^-$. In addition, the virtual photon-parton centre-of-mass energy

$$s_{\gamma^* p} = (k - p_b)^2 = k^+k^- - k^+p_b^- \simeq k^+p_{b'}^- \tag{C.3}$$

is required in the high-energy limit to be much larger than the virtual photon momentum transfer $k^2$, i.e. $s_{\gamma^* p} \gg |k^2|$. This entails that $p_{b'}^- \gg |k^-|$. Thus in the momentum conservation along the minus direction the momentum $k^-$ can be neglected, and we can summarise the momentum conservation in the high-energy limit as

$$\begin{aligned} -p_a^+ - p_{a'}^+ = k^+ &\simeq p_1^+ + p_2^+ \\ -p_b^- &\simeq p_{b'}^- \\ 0 &= p_{1\perp} + p_{2\perp} + p_{b'\perp} . \end{aligned} \tag{C.4}$$

Equaiton (C.4) can be viewed as defining two scattering centres through the + and − momentum conservation, which act independently. The two scattering centres are linked by the transverse momentum conservation only.

Next, we must approximate the exact amplitudes in the high-energy limit. The colour decomposition of the amplitude for $e^+e^- \to q\bar{q}gg$ in the conventions of ref. [35], is

$$\mathcal{A}_6\left(1_q, b, b', 2_{\bar{q}}; a_{\bar{e}}, a'_e\right) = -2e^2 g_S^2 Q_{f_q} \sum_{\sigma \in S_2} (T^{a_{\sigma(b)}} T^{a_{\sigma(b')}})_{i_1 \bar{\imath}_2} A_6\left(1_q, \sigma(b), \sigma(b'), 2_{\bar{q}}; a_{\bar{e}}, a'_e\right) \tag{C.5}$$

with sub-amplitudes[8]

$$\begin{aligned} A_6\left(1^+, b^+, b'^-, 2^-, a^-, a'^+\right) &= \frac{1}{s_{bb'} s_{aa'}} \left[ \frac{\langle b'\,1\rangle\,[1\,b]\,\langle 2\,a\rangle\,\langle b'|(1+b)|a'\rangle}{\langle 1\,b\rangle\, t_{1bb'}} - \right. \\ &\quad - \frac{\langle b'\,2\rangle\,[2\,b]\,[1\,a']\,\langle a|(b'+2)|b\rangle}{[b'\,2]\, t_{bb'2}} - \\ &\quad \left. - \frac{\langle a|(b'+2)|b\rangle \langle b'|(1+b)|a'\rangle}{\langle 1\,b\rangle\,[b'\,2]} \right], \end{aligned} \tag{C.6}$$

$$\begin{aligned} A_6\left(1^+, b^-, b'^+, 2^-, a^-, a'^+\right) &= \frac{1}{s_{bb'} s_{aa'}} \left[ - \frac{[1\,b']^2\,\langle 2\,a\rangle\,\langle b|(1+b')|a'\rangle}{[1\,b]\, t_{1bb'}} + \right. \\ &\quad + \frac{\langle b\,2\rangle^2\,[1\,a']\,\langle a|(b+2)|b'\rangle}{\langle b'\,2\rangle\, t_{bb'2}} + \\ &\quad \left. + \frac{[1\,b']\,\langle b\,2\rangle\,[1\,a']\,\langle 2\,a\rangle}{[1\,b]\,\langle b'\,2\rangle} \right]. \end{aligned} \tag{C.7}$$

The sub-amplitudes (C.6) and (C.7) are symmetric under the exchange

$$1 \leftrightarrow 2\,, \qquad b \leftrightarrow b'\,, \qquad a \leftrightarrow a'\,, \qquad \langle ij\rangle \leftrightarrow [ji]\,. \tag{C.8}$$

Alternatively, the amplitude for $e^+e^- \to q\bar{q}Q\bar{Q}$ can be used,

$$\begin{aligned} \mathcal{A}_6^{\rm tree}\left(1_q, b_{\bar{Q}}, b'_Q, 2_{\bar{q}}; a_{\bar{e}}, a'_e\right) &= -2\,e^2\,g_S^2 \sum_{a=1}^{8} T^a_{i_1\bar{\imath}_2} T^a_{i_{b'}\bar{\imath}_b} \times \\ &\times \left[ Q_{f_q}\, A_6^{\rm tree}\left(1_q, b_{\bar{Q}}, b'_Q, 2_{\bar{q}}; a_{\bar{e}}, a'_e\right) + Q_{f_Q}\, A_6^{\rm tree}\left(b'_Q, 2_{\bar{q}}, 1_q, b_{\bar{Q}}; a_{\bar{e}}, a'_e\right)\right] \end{aligned} \tag{C.9}$$

with sub-amplitude

$$\begin{aligned} & A_6^{\rm tree}\left(1^+, b^+, b'^-, 2^-; a^-, a'^+\right) = \\ & = \frac{1}{s_{bb'} s_{aa'}} \left[ \frac{[1\,b]\,\langle a\,2\rangle\,\langle b'|(1+b)|a'\rangle}{t_{1bb'}} + \frac{\langle b'\,2\rangle\,[a'\,1]\,\langle a|(b'+2)|b\rangle}{t_{bb'2}} \right]. \end{aligned} \tag{C.10}$$

In order to evaluate the sub-amplitudes above, we need to compute the Mandelstam invariants and the spinor products in the high-energy limit. In the virtual photon-parton frame, the three-particle invariants can be written *exactly* as

$$t_{iaa'} = (p_i + p_a + p_{a'})^2 = k^2 - \frac{k^+}{p_i^+}|p_{i_\perp}|^2 - \frac{p_i^+}{k^+}k^2\,, \qquad i = 1, 2\,, \tag{C.11}$$

[8]We use the same sub-amplitudes as in ref. [35], but we ignore the overall factor of $i$. In addition, we have neglected the configuration with like-helicity gluons, since it subleading in the high-energy limit.

where $x_i = p_i^+/k^+$, with $i = 1, 2$, are the momentum fractions of the final-state quarks with respect to the virtual photon. In the high-energy limit, we can fix $x_1 = x$ and $x_2 = 1 - x$, and rewrite the invariants (C.11) as

$$
\begin{aligned}
t_{1aa'} &= t_{2bb'} = (1-x)k^2 - \frac{|p_{1\perp}|^2}{x}\,,\\
t_{2aa'} &= t_{1bb'} = xk^2 - \frac{|p_{2\perp}|^2}{(1-x)}\,.
\end{aligned}
\tag{C.12}
$$

In light-cone coordinates, a generic spinor product can be written as

$$
\langle p_i p_j\rangle = p_{i\perp}\sqrt{\frac{p_j^+}{p_i^+}} - p_{j\perp}\sqrt{\frac{p_i^+}{p_j^+}}\,. \tag{C.13}
$$

In the kinematics (C.4), the spinor products are

$$
\begin{aligned}
\langle p_a p_b\rangle &= -\sqrt{\hat{s}} \simeq -\sqrt{(p_1^+ + p_2^+ + p_{a'}^+)p_{b'}^-}\,,\\
\langle p_a p_{b'}\rangle &= -i\sqrt{\frac{-p_a^+}{p_{b'}^+}}\,p_{b'_\perp} \simeq i\frac{p_{b'_\perp}}{|p_{b'_\perp}|}\langle p_a p_b\rangle\,,\\
\langle p_a p_j\rangle &= i\left((-p_{a_\perp})\sqrt{\frac{p_j^+}{-p_a^+}} - p_{j_\perp}\sqrt{\frac{-p_a^+}{p_j^+}}\right),\\
\langle p_j p_b\rangle &= i\sqrt{-p_b^- p_j^+} \simeq i\sqrt{p_j^+ p_{b'}^-}\,,\\
\langle p_{b'} p_b\rangle &= i\sqrt{-p_b^- p_{b'}^+} \simeq i|p_{b'_\perp}|\,,\\
\langle p_j p_{b'}\rangle &= p_{j_\perp}\sqrt{\frac{p_{b'}^+}{p_j^+}} - p_{b'_\perp}\sqrt{\frac{p_j^+}{p_{b'}^+}} \simeq -p_{b'_\perp}\sqrt{\frac{p_j^+}{p_{b'}^+}}\,,
\end{aligned}
\tag{C.14}
$$

with $j = 1, 2, a'$, and where we have taken the phase conventions of ref. [36]. Momentum conservation (C.4) implies that $p_a^+ = -p_{a'}^+ - p_1^+ - p_2^+$ and $p_{a\perp} = -p_{a'\perp}$.

Using the invariants (C.12) and the spinor products (C.14), the high-energy expansion of eq. (C.5) can be written as

$$
\begin{aligned}
&\mathcal{A}_6\left(1_q^\nu, b^\rho, b'^{\rho'}, 2_{\bar{q}}^{-\nu}, a_{\bar{e}}^{-\lambda}, a'^{\lambda}_{e}\right) = \\
&\quad = 2s_{\gamma^* p}\left[g_S e^2 Q_{f_q}\, T^c_{i_1\bar{\imath}_2}\,\sqrt{2}V_f\left(a_{\bar{e}}^{-\lambda}; a'^{\lambda}_{e}, 1_q^\nu, 2_{\bar{q}}^{-\nu}\right)\right]\frac{1}{t}\left[\frac{i}{\sqrt{2}}g_S f^{bb'c}\, C\left(b_g^\rho; b'^{\rho'}_{g}\right)\right],
\end{aligned}
\tag{C.15}
$$

where $s_{\gamma^* p} \simeq k^+ p_{b'}^-$ is the virtual photon-parton centre-of-mass energy, $t = s_{bb'} \simeq -|p_{b'\perp}|^2 = -|q_\perp|^2$ is the momentum transfer, with $q = p_b + p_{b'}$ the momentum of the gluon exchanged in the crossed channel, and where $\lambda\,, \nu$ and $\rho$ denote the helicity of the lepton pair, the quark pair and the gluons, respectively. Using the impact factor for the gluon vertex, $C(b_g^+; b'^-_{g}) = p_{b'\perp}/p^*_{b'\perp}$, according to the conventions of ref. [36][9] we obtain the impact

[9] In ref. [36] the generators of the group are normalised to 1/2, while in this paper to 1. We introduced the explicit $1/\sqrt{2}$ factor in eq. (C.15) to take into account this difference.

factor for $eg^* \to eq\bar{q}$,

$$V_f(a^-_{\bar{e}}; a'^+_e, 1^+_q, 2^-_{\bar{q}}) = \tag{C.16}$$
$$= -\frac{i}{k^2}\left[\frac{x(1-x)}{-x(1-x)k^2+|p_{2\perp}|^2}\left(p_{a\perp}\sqrt{\frac{p_2^+}{-p_a^+}}+p_{2\perp}\sqrt{\frac{-p_a^+}{p_2^+}}\right)\left(p^*_{2\perp}\sqrt{\frac{p_{a'}^+}{p_1^+}}+p^*_{a'\perp}\sqrt{\frac{p_1^+}{p_{a'}^+}}\right)+\right.$$
$$\left.+\frac{x(1-x)}{-x(1-x)k^2+|p_{1\perp}|^2}\left(p^*_{1\perp}\sqrt{\frac{p_{a'}^+}{p_1^+}}-p^*_{a'\perp}\sqrt{\frac{p_1^+}{p_{a'}^+}}\right)\left(p_{a\perp}\sqrt{\frac{p_2^+}{-p_a^+}}-p_{1\perp}\sqrt{\frac{-p_a^+}{p_2^+}}\right)\right].$$

Note that in eq. (C.16) there is no divergence when the momenta $p_1$ and $p_2$ of the quark pair become collinear. As a check of the calculation (or of high-energy factorisation), we have evaluated also the amplitude (C.9) in the high-energy limit, and have obtained the same result as in eq. (C.15), up to the substitution

$$ig_S\, f^{bb'c}\, C\left(b_g^{\nu_b}; b'^{\nu_{b'}}_g\right) \leftrightarrow g_S\, T^c_{b'\bar{b}}\, C\left(b_{\bar{q}}^{-\nu_{b'}}; b'^{\nu_{b'}}_q\right), \tag{C.17}$$

with impact factor for the quark vertex, $C(b^+_{\bar{q}}; b'^-_q) = (-\mathrm{i})p_{b'\perp}/|p_{b'\perp}|$.

Using discrete symmetries of the helicity amplitudes, we find the impact factors with the helicities of the quark and/or the lepton pairs flipped,

$$\begin{aligned}
V_f\left(a^+_{\bar{e}}; a'^-_e, 1^-_q, 2^+_{\bar{q}}\right) &= \left[V_f\left(a^-_{\bar{e}}; a'^+_e, 1^+_q, 2^-_{\bar{q}}\right)\right]^*,\\
V_f\left(a^-_{\bar{e}}; a'^+_e, 1^-_q, 2^+_{\bar{q}}\right) &= V_f\left(a^-_{\bar{e}}; a'^+_e, 2^+_q, 1^-_{\bar{q}}\right),\\
V_f\left(a^+_{\bar{e}}; a'^-_e; 1^+_q, 2^-_{\bar{q}}\right) &= \left[V_f\left(a^-_{\bar{e}}; a'^+_e; 2^+_q, 1^-_{\bar{q}}\right)\right]^*.
\end{aligned} \tag{C.18}$$

The impact factor for the backward kinematics is

$$V_b\left(a^-_{\bar{e}}; a'^+_e; 1^+_q, 2^-_{\bar{q}}\right) = e^{\mathrm{i}\phi}\, V_f\left(a'^-_{\bar{e}}; a^+_e; 2^+_q, 1^-_{\bar{q}}\right)\Big|_{+\to-}, \tag{C.19}$$

where the phase $e^{\mathrm{i}\phi}$ for us is immaterial since we compute squared amplitudes and the index $+\to-$ means that the plus components in eq. (C.16) are replaced with minus components.

Equation (C.16) can be decomposed further in terms of an impact factor for $\gamma^* g^* \to q\bar{q}$ by factoring the lepton current times the photon propagator $\langle p_a|i\,\gamma^\mu|p_{a'}\rangle(-ig_{\mu\nu})/k^2$,

$$V_f\left(a^-_{\bar{e}}; a'^+_e, 1^+_q, 2^-_{\bar{q}}\right) = \langle a-|\mathrm{i}\gamma^\mu|a'-\rangle \frac{-\mathrm{i}g_{\mu\nu}}{k^2} V^\nu_{\gamma^*}\left(k; 1^+_q, 2^-_{\bar{q}}\right). \tag{C.20}$$

In light-cone notation, the lepton current is

$$\langle p_a-|i\,\gamma^\mu|p_{a'}-\rangle = -2\left(\sqrt{-p_a^+p_{a'}^+},\ \frac{-p_{a\perp}p^*_{a'\perp}}{\sqrt{-p_a^+p_{a'}^+}};\ -p_{a\perp}\sqrt{\frac{p_{a'}^+}{-p_a^+}},\ p^*_{a'\perp}\sqrt{\frac{-p_a^+}{p_{a'}^+}}\right), \tag{C.21}$$

with the $\gamma$ matrices chosen in the chiral representation as in ref. [36]. The impact factor

$V^{\mu}_{\gamma^*}(k; 1_q^+, 2_{\bar{q}}^-)$ for the $\gamma^* g^* \to q^+ \bar{q}^-$ process can be written as

$$V^{\mu}_{\gamma^*}\left(k; 1_q^+, 2_{\bar{q}}^-\right) = \tag{C.22}$$
$$= \frac{\sqrt{x(1-x)}}{-x(1-x)k^2 + |p_{2\perp}|^2} \left(x(1-x)k^+,\, \frac{|p_{2\perp}|^2}{-k^2}k^-;\, xp_{2\perp},\, -(1-x)p^*_{2\perp}\right) -$$
$$- \frac{\sqrt{x(1-x)}}{-x(1-x)k^2 + |p_{1\perp}|^2} \left(x(1-x)k^+,\, \frac{|p_{1\perp}|^2}{-k^2}k^-;\, -xp_{1\perp},\, (1-x)p^*_{1\perp}\right).$$

Using $k = (k^+, k^-; 0_\perp)$, we can easily check that $k_\mu V^{\mu}_{\gamma^*}(k; 1_q^+, 2_{\bar{q}}^-) = 0$.

Finally, if we contract with the polarization vector, $\varepsilon^\mu = (\varepsilon^+,\, \varepsilon^-;\, \varepsilon_\perp)$, of the virtual photon, we obtain

$$V^{\varepsilon}_{\gamma^*}\left(k; 1_q^+, 2_{\bar{q}}^-\right) = \tag{C.23}$$
$$= \frac{\sqrt{x(1-x)}}{-x(1-x)k^2 + |p_{2\perp}|^2} \left(\sqrt{x(1-x)}k^+\varepsilon^- + \frac{|p_{2\perp}|^2}{-k^2}k^-\varepsilon^+ + (1-x)p^*_{2\perp}\varepsilon_\perp - xp_{2\perp}\varepsilon^*_\perp\right) -$$
$$- \frac{\sqrt{x(1-x)}}{-x(1-x)k^2 + |p_{1\perp}|^2} \left(\sqrt{x(1-x)}k^+\varepsilon^- + \frac{|p_{1\perp}|^2}{-k^2}k^-\varepsilon^+ - (1-x)p^*_{1\perp}\varepsilon_\perp + xp_{1\perp}\varepsilon^*_\perp\right).$$

We have checked that using this form of the impact factor, we can reproduce the cross section in the high-energy limit obtained in ref. [25].

The impact factor with the helicity of the quark pair flipped is obtained by exchanging the momenta of the quark and antiquark,

$$V^{\mu}_{\gamma^*}\left(k; 1_q^-, 2_{\bar{q}}^+\right) = V^{\mu}_{\gamma^*}\left(k; 2_q^+, 1_{\bar{q}}^-\right), \tag{C.24}$$

The impact factors for the backward kinematics, $k^- \gg k^+$, have the same functional form as given by eq. (C.22) (up to a phase) with the $+$ and $-$ components as well as the quark helicities interchanged.

As a final check, we computed the impact factor for $eg^* \to eq\bar{q}$, eq. (C.16), also in the electron-parton frame, and verified that it agrees with the colour-subleading piece, termed $B_2$, of the impact factor for $qg^* \to qQ\bar{Q}$, computed in ref. [36].

**Note added in proof.** After the completion of this work, we learned that the ALEPH collaboration has also finished its analysis of double tagged events at LEP to measure the hadronic cross section in virtual photon-photon scattering [37]. In contradiction to the L3 results, this analysis indicates that the NLO QCD prediction is sufficient to describe the data in the high-$Y$ region, but is unable to predict correctly the measured yields in the low-$Y$ region. One has to resolve this apparent contradiction before applying the analysis presented in this paper to the ALEPH selection cuts.

## References


[1] I.I. Balitsky and L.N. Lipatov, *The pomeranchuk singularity in quantum chromodynamics*, *Sov. J. Nucl. Phys.* **28** (1978) 822.

[2] E.A. Kuraev, L.N. Lipatov and V.S. Fadin, *Multi-reggeon processes in the Yang-Mills theory*, *Sov. Phys. JETP* **44** (1976) 443.

[3] E.A. Kuraev, L.N. Lipatov and V.S. Fadin, *The Pomeranchuk singularity in nonabelian gauge theories*, *Sov. Phys. JETP* **45** (1977) 199.

[4] H1 collaboration, S. Aid et al., *The gluon density of the proton at low $x$ from a QCD analysis of $F_2$*, *Phys. Lett.* **B 354** (1995) 494 [hep-ex/9506001].

[5] S. Forte and R.D. Ball, *Double scaling violations*, hep-ph/9607291.

[6] H1 collaboration, S. Aid et al., *Transverse energy and forward jet production in the low $x$ regime at hera*, *Phys. Lett.* **B 356** (1995) 118 [hep-ex/9506012].

[7] ZEUS collaboration, J. Breitweg et al., *Forward jet production in deep inelastic scattering at hera*, *Eur. Phys. J.* **C 6** (1999) 239 [hep-ex/9805016].

[8] H1 collaboration, C. Adloff et al., *Forward jet and particle production at hera*, *Nucl. Phys.* **B 538** (1999) 3 [hep-ex/9809028].

[9] J. Bartels, V. Del Duca, A. De Roeck, D. Graudenz and M. Wusthoff, *Associated jet production at hera*, *Phys. Lett.* **B 384** (1996) 300 [hep-ph/9604272].

[10] E. Mirkes and D. Zeppenfeld, *Forward jet production at desy hera in the low $x$ regime in next-to-leading order*, *Phys. Rev. Lett.* **78** (1997) 428 [hep-ph/9609231].

[11] L.H. Orr and W.J. Stirling, *A BFKL Monte Carlo approach to jet production at hadron-hadron and lepton-hadron colliders*, hep-ph/9804431.

[12] D0 collaboration, S. Abachi et al., *The azimuthal decorrelation of jets widely separated in rapidity*, *Phys. Rev. Lett.* **77** (1996) 595 [hep-ex/9603010].

[13] D0 collaboration, B. Abbott et al., *Probing BFKL dynamics in the dijet cross section at large rapidity intervals in $p\bar{p}$ collisions at $\sqrt{s} = 1800\,GeV$ and $630\,GeV$*, *Phys. Rev. Lett.* **84** (2000) 5722 [hep-ex/9912032].

[14] A.H. Mueller and H. Navelet, *An inclusive minijet cross-section and the bare pomeron in QCD*, *Nucl. Phys.* **B 282** (1987) 727.

[15] V. Del Duca and C.R. Schmidt, *Dijet production at large rapidity intervals*, *Phys. Rev.* **D 49** (1994) 4510 [hep-ph/9311290].

[16] W.J. Stirling, *Production of jet pairs at large relative rapidity in hadron-hadron collisions as a probe of the perturbative pomeron*, *Nucl. Phys.* **B 423** (1994) 56 [hep-ph/9401266].

[17] V. Del Duca and C.R. Schmidt, *BFKL versus $\mathcal{O}\alpha_s^3$ corrections to large rapidity dijet production*, *Phys. Rev.* **D 51** (1995) 2150 [hep-ph/9407359].

[18] L.H. Orr and W.J. Stirling, *The collision energy dependence of dijet cross sections as a probe of bfkl physics*, *Phys. Lett.* **B 429** (1998) 135 [hep-ph/9801304].

[19] J.R. Andersen, V. Del Duca, S. Frixione, C.R. Schmidt and W.J. Stirling, *Mueller-Navelet jets at hadron colliders*, *J. High Energy Phys.* **02** (2001) 007 [hep-ph/0101180].

[20] L3 collaboration, M. Acciarri et al., *Measurement of the cross-section for the process $\gamma^*\gamma^* \to$ hadrons at LEP*, *Phys. Lett.* **B 453** (1999) 333.

[21] OPAL collaboration, G. Abbiendi et al., *Measurement of the hadronic cross-section for the scattering of two virtual photons at LEP*, hep-ex/0110006.

[22] L3 collaboration, P. Achard et al., *Double-tag events in two-photon collisions at LEP*, *Phys. Lett.* **B 531** (2002) 39 [hep-ex/0111012].

JHEP05(2002)005

[23] A.H. Mueller, *Soft gluons in the infinite momentum wave function and the BFKL pomeron*, *Nucl. Phys.* **B 415** (1994) 373.

[24] A.H. Mueller and B. Patel, *Single and double BFKL pomeron exchange and a dipole picture of high-energy hard processes*, *Nucl. Phys.* **B 425** (1994) 471 [hep-ph/9403256].

[25] S.J. Brodsky, F. Hautmann and D.E. Soper, *Virtual photon scattering at high energies as a probe of the short distance pomeron*, *Phys. Rev.* **D 56** (1997) 6957 [hep-ph/9706427].

[26] J. Bartels, A. De Roeck and H. Lotter, *The $\gamma^*\gamma^*$ total cross section and the BFKL pomeron at $e^+e^-$ colliders*, *Phys. Lett.* **B 389** (1996) 742 [hep-ph/9608401].

[27] J. Bartels, C. Ewerz and R. Staritzbichler, *Effect of the charm quark mass on the BFKL $\gamma^*\gamma^*$ total cross section at LEP*, *Phys. Lett.* **B 492** (2000) 56 [hep-ph/0004029].

[28] J.A.M. Vermaseren, *Two photon processes at very high-energies*, *Nucl. Phys.* **B 229** (1983) 347.

[29] M. Cacciari, V. Del Duca, S. Frixione and Z. Trócsányi, *QCD radiative corrections to $\gamma^*\gamma^* \to$ hadrons*, *J. High Energy Phys.* **02** (2001) 029 [hep-ph/0011368].

[30] V.D. Barger, T. Han, J. Ohnemus and D. Zeppenfeld, *Pair production of $W^{\pm}$, $\gamma$ and $Z$ in association with jets*, *Phys. Rev.* **D 41** (1990) 2782.

[31] S. Catani, Y.L. Dokshitzer, M. Olsson, G. Turnock and B.R. Webber, *New clustering algorithm for multi-jet cross-sections in $e^+e^-$ annihilation*, *Phys. Lett.* **B 269** (1991) 432.

[32] Particle Data Group collaboration, D.E. Groom et al., *Review of particle physics*, *Eur. Phys. J.* **C 15** (2000) 1.

[33] T. Stelzer and W.F. Long, *Automatic generation of tree level helicity amplitudes*, *Comput. Phys. Commun.* **81** (1994) 357 [hep-ph/9401258].

[34] F. Richard, J.R. Schneider, D. Trines, and A. Wagner, *Tesla technical design report part 1. Executive summary*, hep-ph/0106314.

[35] Z. Bern, L.J. Dixon and D.A. Kosower, *One-loop amplitudes for $e^+e^-$ to four partons*, *Nucl. Phys.* **B 513** (1998) 3 [hep-ph/9708239].

[36] V. Del Duca, A. Frizzo and F. Maltoni, *Factorization of tree QCD amplitudes in the high-energy limit and in the collinear limit*, *Nucl. Phys.* **B 568** (2000) 211 [hep-ph/9909464].

[37] ALEPH collaboration, A. Heister et al., *Measurement of the hadronic cross section of doubletagged $\gamma\gamma$ events at ALEPH*, contribution to the PHOTON01 Conference.